Indoor Optical Wireless Power Transfer to Small Cells at Nighttime

Indoor Optical Wireless Power Transfer to Small Cells at Nighttime

John Fakidis, *Student Member, IEEE,* Stefan Videv, Stepan Kucera, *Senior Member, IEEE,* Holger Claussen, *Senior Member, IEEE,* and Harald Haas, *Member, IEEE*

***Abstract*—The application of wireless backhaul communication and power transfer to outdoor small cells (SCs) could significantly decrease their installation cost. In this paper, the concept of indoor optical wireless power transfer (OWPT) to SCs is investigated in the absence of ambient light, i.e. during darkness hours. An experimental study is conducted by the use of up to 4 red laser diodes (LDs), a crystalline silicon (c-Si) solar panel and cell placed at $5.2\,$m. A value of 69% is measured for the fill factor (FF) of the solar panel. Also, a total power efficiency of 3.2% is measured for an optical wireless (OW) link with an average efficiency of 2 LDs of 26.8%, a solar cell efficiency of 13.3% and only 10.6% of geometrical losses. A comparison of this link with a state-of-the-art inductive power transfer system (IPTS) shows an improvement of the total link efficiency by 2.7 times. Another OW link is implemented with a divergence of full width at 36.8% of the peak intensity of $3\,$mrad and $5.75\,$mrad along the small and large axes of the beam, respectively. The experimental levels of harvested power are in the order of mW, whereas approximately $1\,$W is required for the operation of a SC. Therefore, a 42 laser-based transmitter is designed both analytically and by the use of the simulation tool Zemax. The respective results show the feasibility of delivering $7.2\,$W of optical power to a solar cell of up to $30\,$m distance with geometrical losses of only 2%, but a beam enclosure is also required due to eye safety restrictions.**

***Index Terms*—Small cells (SCs), optical wireless power transfer (OWPT), energy harvesting (EH), radio frequency (RF), rectennas, diode lasers, quantum well lasers, laser beams, solar energy, energy efficiency.**

I. Introduction

THE principle of small cells (SCs) is widely accepted as one of the solutions with most potential to the exponential increase in capacity demand of heterogeneous mobile networks [1]. Despite the fact that a large scale outdoor deployment of SCs offers advantages such as high network capacity [2] and reduced power consumption [3], the high installation cost is the most restrictive factor. The technology of optical fibers is considered to be one of the potential solutions to the provision of high speed backhaul communication to SCs [4]. However, the main disadvantages are the installation cost and the requirement for a mains power supply. Therefore, alternative sources of power supply and wireless backhaul communication can make the deployment of SCs more cost effective.

The concept of energy harvesting (EH) or power harvesting (PH) from natural resources, such as sun and wind, [5] as an alternative source of power supply has the main disadvantage of the variability of weather conditions. Therefore, the technology of wireless power transfer (WPT) from artificial electromagnetic (EM) sources has been proposed as a complementary and reliable solution. The concept of WPT was inspired and demonstrated for the first time by Nikola Tesla in the late 19^{th} century using a radio frequency (RF) resonant transformer, termed a Tesla coil [6]. The application of WPT is also feasible using devices operating at the visible light (VL) and infra-red (IR) part of the EM spectrum, such as laser diodes (LDs) or light-emitting diodes (LEDs) and solar cells. The concept in the optical domain is termed optical wireless power transfer (OWPT).

The research field of optical wireless communications (OWC) has been proposed as a complementary technology to RF data communication and as a potential solution to the exponential increase in demand for wireless data transmission [7]. The broad research field of OWC can be separated into two parts: free space optical (FSO) communications and visible light communications (VLC). Free space optical systems mostly comprise coherent data transmission using lasers at the transmitter and photodiodes (PDs) at the receiver. Also, FSO systems are usually deployed outdoors covering distances of several kilometers. Visible light communications facilitate the use of LEDs and PDs and are mainly applied to indoor public places such as offices, conference venues, museums, hotels and hospitals.

The objective is to investigate the simultaneous application of OWPT for the provision of $1\,$W and high speed FSO backhaul communication to outdoor SCs. However, as a first step, in this comprehensive study, research is focused on the indoor OWPT to SCs at nighttime. The conditions of darkness are selected because the system should also work when there is no ambient light to harvest. A set of three studies is reported in this paper. In Study I, a small number of LDs is used for optical power transmission in the order of mW to observe how the solar receiver efficiency scales with the input optical power. According to that result and a physical model, an estimation of the number of LDs required to achieve $1\,$W of harvested power is made. However, since the experimental distance in Study I is only $5.2\,$m and the concept of power supply to SCs refers to practical link distances of $100\,\text{m}-300\,\text{m}$, we need to affirm that the optical wireless (OW) link operates at longer distances. For this reason, Study II is undertaken for

Part of this work was presented at the *IEEE Int. Conf. Commun. (ICC) Workshops*, London, UK, Jun. 8, 2015.

J. Fakidis, S. Videv and H. Haas are with the Li-Fi Research and Development Centre, Institute for Digital Communications, School of Engineering, University of Edinburgh, Edinburgh, EH9 3JL, UK (e-mail: {j.fakidis, s.videv, h.haas}@ed.ac.uk).

S. Kucera and H. Claussen are with Bell Laboratories, Nokia, Blanchardstown Business & Technology Park, Dublin 15, Ireland (e-mail: {stepan.kucera, holger.claussen}@nokia.com).

the determination of laser beam divergence. A targeted beam divergence of 1 mrad is considered because the beam diameter is only 10 cm at 100 m, assuming the LD to be a point source. Therefore, the geometrical losses of such a laser link could be compensated by the use of a receiver with a large aperture. The estimated number of LDs required for harvesting 1 W is 61, as shown in Study I. Therefore, in Study III a multiple laser transmitter is designed to transfer wirelessly 7.2 W of optical power to the solar cell that achieved the highest efficiency in Study I. However, in Study III a number of 42 LDs with collimation lenses are simulated, since they transmit higher levels of power than the LDs considered in Study I.

1) Study I – Total Link and Components Efficiency: The implemented OWPT links operate at a distance of 5.2 m in order to compare metrics of electrical performance (such as total power efficiency and harvested power) with the respective parameters measured in [8]–[10]. A solar panel and a single solar cell are used in the experiments. Also, a physical model is developed for the propagation of an elliptical Gaussian beam through a lens to free space and is used to obtain the laser classification and to determine the irradiance limits for eye safety [11]. An effective single diode physical model of the solar panel [12] is presented and applied to the experimental data for curve fitting. Most importantly, the analytical models are used to estimate the number of optical transmitters required to achieve 1 W of harvested power. Since the total link efficiency is a function of the efficiency of the components, the efficiency of the LDs and solar cell is measured to determine the geometrical losses. The performance of this link in terms of total efficiency is fairly compared with a state-of-the-art inductive power transfer system (IPTS) with optimally shaped dipole coils [10]; this shows an improvement by 2.7 times. The maximum harvested power is measured to be only 25.7 mW; and an estimated number of 61 LDs and lenses is shown to be required for harvesting 1 W.

2) Study II – Laser Beam Collimation: In Study II, a single LD is used with a large lens for light collimation. Also, the physical model of the Gaussian beam propagation developed in Study I is applied to the experimental measured points of irradiance. Thus, divergence values of full width at 36.8% of the peak intensity of 3 mrad and 5.75 mrad are reported along the small and large axes of the beam, respectively. Therefore, it can be concluded that the developed OW link is capable of transmitting power efficiently at long distances, such as 100 m−300 m.

3) Study III – Harvested Power with a Targeted Value of 1 W: In Study III, the feasibility of harvesting 1 W is investigated using a simulation framework in Zemax and the respective analytical model of multiple elliptical Gaussian beams developed in Study I. Although 61 LDs with a typical output power of 50 mW for each diode are shown to be required for harvesting 1 W in Study I, LDs with typical output power of 171 mW for each diode are considered in Study III. In particular, an array of 42 LDs and lenses is created with the capability of transmitting 7.2 W to the solar cell that achieved the highest efficiency in Study I up to 30 m. The geometrical losses of this multiple link are calculated to be only 2% based on the simulation and analytical model, and both are in close agreement. However, enclosure of the laser beams is required due to eye safety restrictions.

The rest of the paper is organized as follows: in Section II, a literature review is given. In Section III, the study of total link and components efficiency is provided. In Section IV, the study of laser beam collimation is given. In Section V, the study of harvesting 1 W is provided. Finally, concluding comments are given in Section VI.

II. Previous Work

Tesla's pioneering work has attracted research interest mostly in the RF and more specifically in the micro-wave (μ-wave) region of the EM spectrum [13], [14]. The basic methods of WPT are near field magnetic resonance coupling [15], [16]; inductive coupling [10], [17]; far field RF or μ-wave power transfer [18], [19]; and power transmission from laser sources [20], [21].

A. Radio Frequency Based Wireless Power Transfer

In [15], a strongly coupled magnetic resonance system (CMRS) was implemented and had the capability of transferring the amount of 60 W up to a distance of 2 m with an overall wall-to-load efficiency of 15%. Also, in [17], the transfer of 105 W at a distance of 30 cm was demonstrated by the use of an IPTS with a direct current (DC)-to-load efficiency of 77%. However, so long as the outdoor installation of SCs requires a harvested amount of electrical power of 1 W at relatively long link distances in the order of 100 m−300 m, the only potential solutions are considered to be the techniques of wireless power transmission from RF or μ-wave antennas and laser sources [13].

The EH functionality of RF or μ-wave radiation is executed by a diode-based circuit, termed as rectenna [13], [22]. The rectenna consists of a rectifying circuit and a receiving antenna for the conversion of the input RF or μ-wave power to DC power. In [13], an overview of the state-of-the-art measured values of rectenna efficiency ranging from 1.2% to 90.6% was presented. However, the results of total link efficiency and distance were not reported. Note that rectennas are exclusively designed to harvest either ambient RF power in the order of a few μW [23] or RF power from 'dedicated' antennas [24]. Thus, they do not have the ability to harvest power from a natural resource.

B. Optical Wireless Power Transfer and Energy Harvesting from Sunlight

The concept of OWPT based on laser sources was first introduced for the application of solar power satellite (SPS) [20], [25]. Current research developments in the technology of high power LDs report levels of output optical power greater than 10 W with a respective conversion efficiency more than 65% in the wavelength region of 940 nm−980 nm [26]. Also, the use of passive optical elements for light collimation, such as lenses, creates uncomplicated laser systems of very high directivity. In addition to this important characteristic, the wide availability of outdoor solar panels presents the unique potential of PH both from ambient light, where sunlight is included, and from 'dedicated' laser sources establishing the

principle of OWPT. Moreover, high levels of irradiance of $100\,\text{mW/cm}^2$ are received from sunlight under standard test conditions (STC) [27].

In [28], consolidated tables with reported efficiency values of solar cells and modules measured at STC are given. In particular, the modules of amorphous silicon (a-Si) have an efficiency of 12.3%. Also, the inexpensive technologies of monocrystalline silicon (mono-c-Si) cells and multi-crystalline silicon (multi-c-Si) modules have an efficiency in the order of 25.6% and 18.5%, respectively. The best efficiency values are reported for the technology of concentrator photovoltaics (CPV) that is based on multi-junction cells [29]. A maximum efficiency of 45.7% of a multi-junction cell with a concentrator is reported in [28].

The exclusive indoor application of OWPT was studied in [8] and [9]. In these studies, ambient light was ensured to be negligible and therefore the concept of OWPT to SCs was investigated for dark conditions. In [8], an OW link was created by the use of a high brightness white LED (WLED), a large parabolic mirror for light collimation and an a-Si solar panel placed at $5\,\text{m}$. The maximum measured link efficiency and harvested power were only 0.1% and $18.3\,\text{mW}$, respectively. This fact was attributed to significant geometrical optical losses and very low energy efficiency of the a-Si technology of the panel. The serious geometrical losses of optical power stemmed from the Lambertian radiation pattern of the LED which was the major obstacle for efficient light collimation. Consequently, the next step was the use of highly directive laser sources and a different type of solar panel.

In the follow-up study [9], the OW link was implemented with 1 to 5 red LDs with respective collimation lenses and a multi-c-Si solar panel located at $5.2\,\text{m}$. The maximum measured link efficiency and harvested power using 5 LDs with lenses were only 0.74% and $10.4\,\text{mW}$, respectively. The low levels of link efficiency were attributed to the low LD efficiency and low solar panel efficiency. Also, the low amount of harvested power was explained by the low transmitted optical power and the effect of mismatch losses among cells of the same panel.

C. Simultaneous Wireless Communication and Power Transfer

The practical feasibility of simultaneous EH and data communication by a rectenna was demonstrated in [30] and [31]. In [30], an axial ratio bandwidth of 12.1% and a rectenna efficiency of 57.3% were reported for a link distance of only $35\,\text{cm}$. In [31], a rectenna efficiency of 63% was measured with an input power of $25\,\text{mW}$ operating at $5.78\,\text{GHz}$ for a link distance of $80\,\text{cm}$.

The data transfer using VLC systems has been investigated broadly [32], [33] and the feasibility of a data rate of $3\,\text{Gb/s}$ by a LED source was demonstrated in [34]. Most importantly, the simultaneous use of a solar panel both for PH in the order of mW and high speed OWC with a data rate of $12\,\text{Mb/s}$ was demonstrated in [35] for link distances of up to $95\,\text{cm}$. Also, the same concept was realized in [36], but with the use of a small solar cell capable of harvesting $1\,\text{mW}$ of power and receiving data with a rate of only $3\,\text{kb/s}$.

Since the research objective is to achieve high speed FSO backhaul communication and power transfer to outdoor SCs, a review of the constraints imposed by an atmospheric channel and the potential solutions is given below.

1) Challenges Induced by an Atmospheric Channel: Laser beam propagation through an atmospheric channel is constrained by factors such as atmospheric attenuation, scintillation, misalignment and ambient light noise [37]. Atmospheric attenuation causes power reduction of the optical waves. It is presented in the form of absorption by gas molecules and Rayleigh and Mie scattering by gas molecules or aerosol particles that are suspended in the air and exist in fog, rain, clouds, smoke and dust [38]. The term scintillation, also known as atmospheric turbulence, is used to describe the random changes in light intensity caused by variations in the refractive index of the atmosphere [38]. Since highly directive laser beams are applied in FSO systems, precise alignment between the transmitter and receiver is required for the maximum possible collection of optical power by the detector. Finally, ambient light, where sunlight is included, can affect the signal-to-noise ratio (SNR) at the receiver, as it is detected in the form of shot noise.

2) Potential Solutions to the Atmospheric Channel's Constraints: Atmospheric losses under clear weather conditions are considered to be negligible and, in this case, only geometrical losses are dominant [39]. Note that a FSO link may become unavailable under heavy fog conditions, but these conditions occur rarely and depend on the local topography and wind conditions. In addition, even under such worst-case weather conditions, multiple FSO links can be created by a number of transmitters and receivers applying the maximal ratio combining (MRC) technique for the selection of the best channel. The scintillation effect results in fading, i.e. temporal and spatial fluctuations of the optical and therefore electrical power of the received signal. The negative effects of scintillation can be alleviated using the method of aperture averaging [40]. Also, the use of a multi-element receiver, such as a solar panel, and relatively large optical devices, such as mirrors, for light collimation and reception are the most efficient ways to address misalignment problems. Therefore, the use of a large aperture at the receiver is considered to be an effective mitigation technique of the effects of scintillation and misalignment. In data communication, while a typical photodetector can be driven to saturation from excessive amounts of ambient light, a solar receiver is more resilient to large amounts of received optical power. Also, since ambient light presents slow variations in time, it can be totally removed either by the use of optical filters or other advanced detection techniques. Finally, the presence of ambient light is an important advantage for EH, as the solar receiver is able to harvest energy not only from 'dedicated' laser sources, but also from the natural resource, i.e. sunlight.

III. Study I: Total Link and Components Efficiency

The objectives, methods, setups, applied analytical models and results of Experiments I–III of Study I are summarized in Table I.

TABLE I
SUMMARY OF EXPERIMENTS IN STUDY I

Study I		Total link and components efficiency			
Experiment		I		II	III
Objective		Determination of maximum fill factor, link efficiency and harvested power		Determination of each laser diode efficiency	Determination of solar receiver efficiency
Method		Measurement of 21 values pairs of load voltage and current		Measurement of output power for 22 values of input power	Measurement of 25 values of received optical power
Setup		Scenario I	Scenario II		
	Optical source	$1-4$ Laser diodes	$1-3$ Laser diodes	Single laser diode	2 Laser diodes
	Optics	$1-4$ Aspheric lenses	$1-3$ Aspheric lenses	-	2 Aspheric lenses
	Receiver	Solar panel	Solar cell	Optical power sensor	Solar cell
	Measurement device	Multimeters		Optical power sensor	Optical power sensor
	Link distance	5.2 m		1.5 mm	5.2 m
Analytical model		(33)–(41)		Quadratic curve fitting*	-
Results		$f_{\text{sr}} = 69\%$ $\eta_{\text{max}} = 2.7\%$ $P_{\text{m}} = 30.6\,\text{mW}$	$f_{\text{sr}} = 54.2\%$ $\eta_{\text{max}} = 3.2\%$ $P_{\text{m}} = 25.7\,\text{mW}$	$\eta_{\text{LD}}^{**} = \{28.1\%, 30.2\%, 32.2\%, 32.9\%\}$	$\eta_{\text{sr}} = 13.3\%$

*No physical model is applied to the experimental data, but two mathematical quadratic polynomials are used.
**Maximum values.

A. Objective

The objective of Study I is to increase the experimental energy efficiency of the 5 m OW link created in [8] and [9]. This is achieved by a decrease in the dimensions, number of cells and a different technology use of the solar receiver in [8] and [9]. An increased maximum link efficiency reduces the number of optical transmitters (i.e. LDs and collimation lenses) required to achieve a harvested electrical power of 1 W. Since each component contributes to the total link efficiency, the efficiency of every single component is determined.

B. Analytical Model

The analytical models of the generated laser beam from the diode, thick lens, reshaped beam from the lens, solar panel and efficiency of total link and components are given below.

An elliptical Gaussian model is considered for the laser beam generated from the diode and the reasoning for this is given in Appendix A. A geometrical illustration of a Gaussian beam is shown in Fig. 1 on the x-z and y-z planes, respectively. When a Gaussian beam passes through any circularly symmetric optical component aligned with the optical beam axis, the Gaussian beam remains Gaussian so long as the paraxial approximation holds for the system [41]. Paraxial approximation is defined in Appendix A. The geometrical parameters and the intensity characteristics of the Gaussian beam emitted from the LD are modified by the geometrical and optical properties of the lens. Therefore, the beam parameters are calculated at four different transverse planes, namely, the emission rectangular area of the LD; the vertices of the input and output surfaces of the aspheric lens; and the positions of the new beam waists along the x- and y- axes, respectively.

1) Generated Beam from the Laser Diode: The LDs used in this study have a multi-quantum well (MQW) structure. The emission rectangular layers of the junction placed inside the packages of the LDs have an area of $(2W_{0\text{x}}) \times (2W_{0\text{y}})$ [42]. Parameters $W_{0\text{x}}$ and $W_{0\text{y}}$ denote the beam waists along the x- and y- axes, respectively. They are calculated from the far field relative intensity patterns as a function of the angular divergences [43], [44]. In particular, the beam waists generated from the LD ($z = 0$) are given by [41]:

$$W_{0\text{x}} = \frac{\lambda_0}{\pi \tan(\vartheta_{\text{x}})} \approx \frac{\lambda_0}{\pi \vartheta_{\text{x}}} \tag{1}$$

and

$$W_{0\text{y}} = \frac{\lambda_0}{\pi \tan(\vartheta_{\text{y}})} \approx \frac{\lambda_0}{\pi \vartheta_{\text{y}}}. \tag{2}$$

The symbol λ_0 denotes the LD operating wavelength, and ϑ_{x} [rad] and ϑ_{y} [rad] represent the perpendicular and parallel to the junction beam divergences. The values of ϑ_{x} and ϑ_{y} correspond to the half width at half maximum (HWHM) intensity points of the Gaussian graphs [43], [44]. The selection of the HWHM beam divergence values is made for the applicability of the paraxial approximation. However, note that the beam divergence of a Gaussian beam can also be defined according to the $1/e \simeq 0.368$ and $1/e^2 \simeq 0.135$ of peak intensity points [37], [45]. It is considered that the optical beam passes from the package aperture of the LD without any optical losses. Also, it is assumed that the protective glass window placed at the front surface of the LD package does not affect the intensity characteristics of the optical beam generated from the MQW source [43], [44]. Therefore, diffraction effects from the circular aperture of the LD are not considered here. This is explained by the Gaussian form of beam intensity shown in the respective LD data sheets [43], [44] instead of the form of a Bessel beam characterized by side lobes [41].

The beam radii along the x- and y- axes can be expressed as a function of distance from the emission area of the LD by [41]:

$$W_{\text{x}}(z) = W_{0\text{x}} \sqrt{1 + \left(\frac{z}{z_{0\text{x}}}\right)^2} \tag{3}$$

and

$$W_{\text{y}}(z) = W_{0\text{y}} \sqrt{1 + \left(\frac{z}{z_{0\text{y}}}\right)^2}, \tag{4}$$

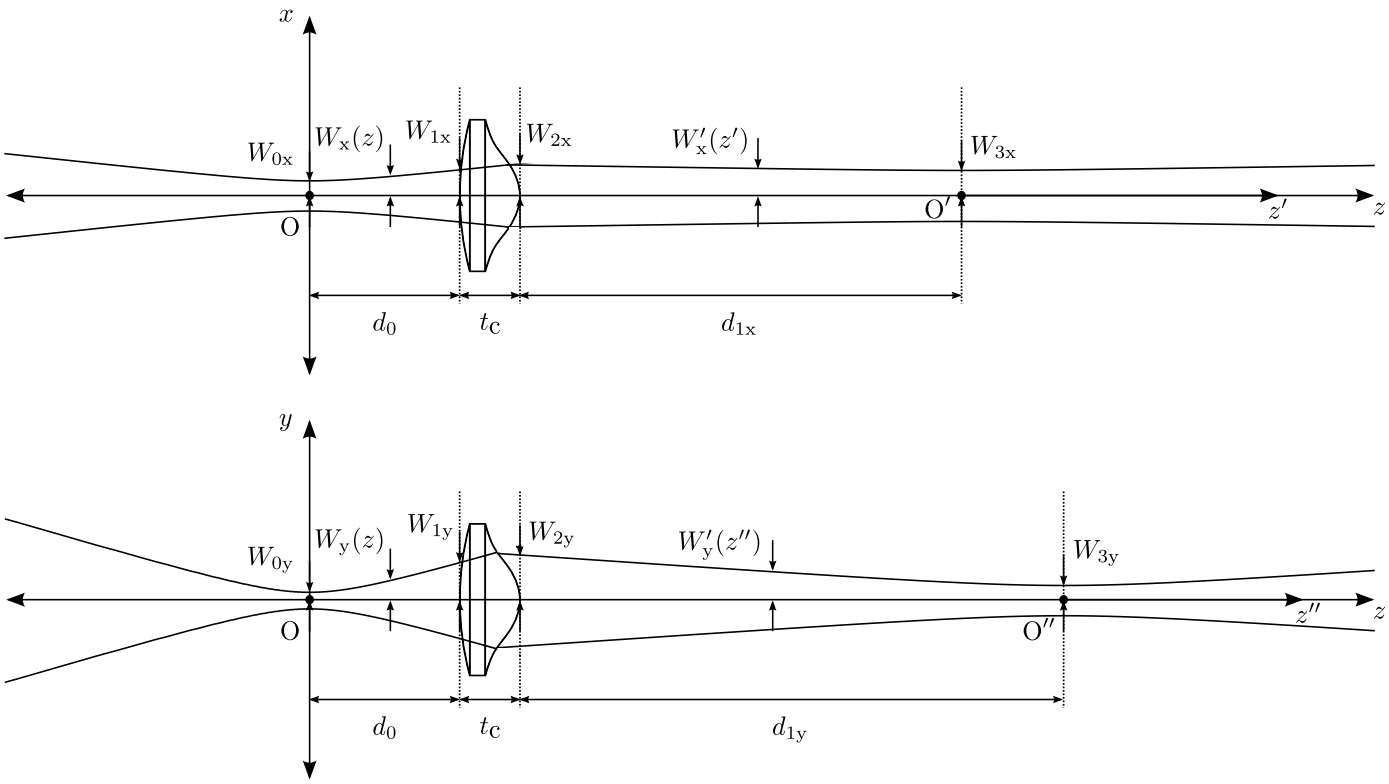

Fig. 1. Geometrical representation of the elliptical Gaussian beam transmitted through an aspheric lens along the x- and y- axes.

where $0 \leq z \leq d_0$; and d_0 denotes the distance between the cross section of the emission source and the tangent plane to the input surface of the lens. Also, z_{0x} and z_{0y} represent the Rayleigh range of the LD beam along the x- and y-directions, respectively. The Rayleigh range is defined as the axial distance between the beam waist and the point where the beam radius is increased by a multiplication factor of $\sqrt{2}$ from its minimum value. These parameters are given by $z_{0x} = \pi W_{0x}^2/\lambda_0$ and $z_{0y} = \pi W_{0y}^2/\lambda_0$ [41].

The beam radii at the tangent plane to the input surface of the lens ($z = d_0$) along the x- and y- axes are calculated by:

$$W_{1x} = W_x(d_0) \overset{(3)}{=} W_{0x}\sqrt{1 + \left(\frac{d_0}{z_{0x}}\right)^2} \tag{5}$$

and

$$W_{1y} = W_y(d_0) \overset{(4)}{=} W_{0y}\sqrt{1 + \left(\frac{d_0}{z_{0y}}\right)^2}. \tag{6}$$

The radii of curvature at $z = d_0$, of the Gaussian beam generated from the LD along the x- and y- axes are given by [41]:

$$R_{1x} = d_0\left[1 + \left(\frac{z_{0x}}{d_0}\right)^2\right] \tag{7}$$

and

$$R_{1y} = d_0\left[1 + \left(\frac{z_{0y}}{d_0}\right)^2\right]. \tag{8}$$

The q- parameters of the Gaussian beam at $z = d_0$ in the x- and y- directions are described by [41]:

$$\frac{1}{q_{1x}} = \frac{1}{R_{1x}} - j\frac{\lambda_0}{\pi W_{1x}^2} \tag{9}$$

and

$$\frac{1}{q_{1y}} = \frac{1}{R_{1y}} - j\frac{\lambda_0}{\pi W_{1y}^2}, \tag{10}$$

where $j = \sqrt{-1}$ is the imaginary unit.

The optical intensity or irradiance, G, of the generated elliptical Gaussian beam in the Cartesian coordinate system, (x, y, z), is expressed as follows [41]:

$$G(x,y,z) = G_0\frac{W_{0x}W_{0y}}{W_x(z)W_y(z)} \times \times \exp\left\{-2\left[\frac{x^2}{W_x^2(z)} + \frac{y^2}{W_y^2(z)}\right]\right\}, \tag{11}$$

where $0 \leq z \leq d_0$; and $G_0 = G(0,0,0)$ is the overall peak intensity.

The total optical power, $P_{\text{Tx,o}}$, of the generated beam is computed at a distance of $0 \leq z \leq d_0$ by [41]:

$$P_{\text{Tx,o}} = \frac{\pi}{2}G_0 W_{0x}W_{0y}. \tag{12}$$

The proof of (12) is presented in Appendix B. Combining (11) and (12), the laser beam intensity can be described as a function of $P_{\text{Tx,o}}$ by:

$$G(x,y,z) = \frac{2P_{\text{Tx,o}}}{\pi W_x(z)W_y(z)} \times \times \exp\left\{-2\left[\frac{x^2}{W_x^2(z)} + \frac{y^2}{W_y^2(z)}\right]\right\}. \tag{13}$$

2) Thick Lens: A method to relate the input and output of an optical system is the use of ray transfer or $ABCD$ matrices [46]. The method of $ABCD$ matrices is also widely used in μ-wave communications [47]. In matrix optics, a simple 2×2 matrix connects the position and angle of paraxial rays at the input and output plane of an optical system through linear algebraic equations. Note that the application of the $ABCD$ law to a Gaussian beam connects the q- parameters of the beam [41]. The diameter of the lens is represented by Δ to avoid any confusion with D, the last element of an $ABCD$ matrix.

The rear surface of the aspheric lens is considered to be spherical. This assumption provides a worst-case scenario for the lens model in terms of light collimation. The elements of an $ABCD$ matrix for a thick lens with two spherical surfaces of different radii of curvature are [48]:

$$A = 1 - \frac{t_{\rm c}(n-1)}{nR_1}, \tag{14}$$

$$B = \frac{t_{\rm c}}{n}, \tag{15}$$

$$C = -(n-1)\left(\frac{1}{R_1} - \frac{1}{R_2}\right) - \frac{t_{\rm c}(n-1)^2}{nR_1R_2}, \tag{16}$$

$$D = 1 + \frac{t_{\rm c}(n-1)}{nR_2}. \tag{17}$$

The parameters $t_{\rm c}$ and n represent the thickness and the refractive index of the lens, respectively. Also, R_1 and R_2 are the radii of the input and output surface of the lens, respectively. The q- parameters of the beam for the x- and y- axes at $z = d_0$ and $z = d_0 + t_{\rm c}$ are connected through the relationships [41]:

$$q_{2\rm x} = \frac{Aq_{1\rm x} + B}{Cq_{1\rm x} + D} \tag{18}$$

and

$$q_{2\rm y} = \frac{Aq_{1\rm y} + B}{Cq_{1\rm y} + D}. \tag{19}$$

Also, the q- parameters of the beam at $z = d_0 + t_{\rm c}$ are given by:

$$\frac{1}{q_{2\rm x}} = \frac{1}{R_{2\rm x}} - j\frac{\lambda_0}{\pi W_{2\rm x}^2} \tag{20}$$

and

$$\frac{1}{q_{2\rm y}} = \frac{1}{R_{2\rm y}} - j\frac{\lambda_0}{\pi W_{2\rm y}^2}. \tag{21}$$

Parameters $W_{2\rm x}$ and $W_{2\rm y}$ represent the beam radii along the x- and y- axes at the tangent plane to the output surface of the lens ($z = d_0 + t_{\rm c}$). Also, $R_{2\rm x}$ and $R_{2\rm y}$ denote the radii of curvature of the reshaped Gaussian beam from the lens at $z = d_0 + t_{\rm c}$. Then, all of these quantities can be calculated from:

$$R_{2\rm x} = \frac{1}{\mathrm{Re}\{1/q_{2\rm x}\}}, \tag{22}$$

$$R_{2\rm y} = \frac{1}{\mathrm{Re}\{1/q_{2\rm y}\}}, \tag{23}$$

$$W_{2\rm x} = \sqrt{-\frac{\lambda_0}{\pi \mathrm{Im}\{1/q_{2\rm x}\}}} \tag{24}$$

and

$$W_{2\rm y} = \sqrt{-\frac{\lambda_0}{\pi \mathrm{Im}\{1/q_{2\rm y}\}}}. \tag{25}$$

Operators $\mathrm{Re}\{.\}$ and $\mathrm{Im}\{.\}$ represent the real and imaginary parts of $1/q_{2\rm x}$ and $1/q_{2\rm y}$, and are calculated by (18) and (19), respectively.

3) Reshaped Beam from the Lens: The distance between the reshaped beam waists and the tangent plane to the output surface of the lens in the x- and y- direction are $d_{1\rm x}$ and $d_{1\rm y}$, respectively. These values of distance can be computed by [41]:

$$d_{1\rm x} = -\frac{R_{2\rm x}}{1 + \left[\lambda_0 R_{2\rm x}/\left(\pi W_{2\rm x}^2\right)\right]^2} \tag{26}$$

and

$$d_{1\rm y} = -\frac{R_{2\rm y}}{1 + \left[\lambda_0 R_{2\rm y}/\left(\pi W_{2\rm y}^2\right)\right]^2}. \tag{27}$$

Also, the waists of the reshaped Gaussian beam, $W_{3\rm x}$ and $W_{3\rm y}$, are given by [41]:

$$W_{3\rm x} = \frac{W_{2\rm x}}{\sqrt{1 + \left[\pi W_{2\rm x}^2/\left(\lambda_0 R_{2\rm x}\right)\right]^2}} \tag{28}$$

and

$$W_{3\rm y} = \frac{W_{2\rm y}}{\sqrt{1 + \left[\pi W_{2\rm y}^2/\left(\lambda_0 R_{2\rm y}\right)\right]^2}}, \tag{29}$$

along the x- and y- axis, respectively.

Now, the reshaped beam radius along the x- axis can be expressed as a function of distance from the vertex of output surface of the lens by:

$$W'_{\rm x}(z') = W_{3\rm x}\sqrt{1 + \left(\frac{z'}{z_{3\rm x}}\right)^2}, \tag{30}$$

where $z' = z - d_0 - t_{\rm c} - d_{1\rm x} \geq -d_{1\rm x}$ is a substituted variable for distance, and $z_{3\rm x} = \pi W_{3\rm x}^2/\lambda_0$ is the Rayleigh range along the x- axis. Similarly, the reshaped beam radius along the y- direction is given as a function of distance from the vertex of output surface of the lens by:

$$W'_{\rm y}(z'') = W_{3\rm y}\sqrt{1 + \left(\frac{z''}{z_{3\rm y}}\right)^2}, \tag{31}$$

where $z'' = z - d_0 - t_{\rm c} - d_{1\rm y} \geq -d_{1\rm y}$ is another substituted variable for distance, and $z_{3\rm y} = \pi W_{3\rm y}^2/\lambda_0$ is the Rayleigh range along the y- axis.

The reshaped Gaussian beam intensity can be computed according to (13) by:

$$G'(x,y,z) = \frac{2(1-r)P_{\rm Tx,o}}{\pi W'_{\rm x}(z')W'_{\rm y}(z'')} \times \exp\left\{-2\left[\frac{x^2}{W'^2_{\rm x}(z')} + \frac{y^2}{W'^2_{\rm y}(z'')}\right]\right\}, \tag{32}$$

where $z \geq d_0 + t_{\rm c}$ and r denotes the reflectance of the lens.

4) Physical Model of Solar Panel and Curve Fitting: In [12], a single diode-based physical model of a solar panel consisting of N_c cells connected in series was proposed. The physical equivalent circuit of that model is shown in Fig. 2. A variable resistor, R_L, is also connected to the output branch, HH', of the solar receiver. Parasitic resistance effects of this photovoltaic (PV) panel are modeled by an effective series resistance, $R_{S,eff}$, and an effective shunt resistance, $R_{P,eff}$. The main factors that contribute to the series resistance generation are the current flow across the p-n junction of the cells; the contact resistance between the metallic grid and the semiconductor; and the resistance between the top and rear metallic contacts. The shunt resistance is caused mainly by manufacturing imperfections rather than a flawed design of solar cells.

The application of Kirchhoff's current law (KCL) to the circuit node F in Fig. 2 gives:

$$I_D - I_P - I_{Ph,eff} + I_L = 0, \tag{33}$$

where I_D is the forward current of the diode; I_P is the parallel current to the source flowing through the branch $F'F$; $I_{Ph,eff}$ is the effective generated photocurrent; and I_L denotes the load current. The current I_D is given by the Shockley diode equation [12]:

$$I_D = I_{0,eff}\left\{ \exp\left[\frac{q}{A_{eff}k_B T}\left(V_L - R_{S,eff}I_L\right)\right] - 1\right\}. \tag{34}$$

The value of $I_{0,eff}$ represents the effective dark saturation current of the diode. The physical constants $q = 1.602 \times 10^{-19}$ C and $k_B = 8.617 \times 10^{-5}$ eV/K denote the electron charge and Boltzmann constant, respectively. The temperature of the PV panel is assumed to be $T = 298$ K. The quantities A_{eff} and V_L represent the effective ideality factor of the diode and the load voltage, respectively. According to Kirchhoff's voltage law (KVL), the current I_P is computed by:

$$I_P = \frac{V_L - R_{S,eff}I_L}{R_{P,eff}}. \tag{35}$$

A transcendental relationship connects the load current and load voltage. This is observed by the substitution of I_D for the second part of (34) and I_P for the second part of (35) in (33). Transcendental equations have only approximate numerical solutions and do not have closed form solutions. The electrical power, P_L, harvested from the load resistor is given by $P_L = V_L I_L$.

This particular model has two measurable parameters, I_L and V_L, and five unknown parameters, $I_{0,eff}$, $R_{S,eff}$, A_{eff}, $R_{P,eff}$ and $I_{Ph,eff}$. These parameters are strongly dependent on the values of optical power incident on the panel. An estimation method of the five unknown parameters is followed by the application of a simple exhaustive search algorithm with discrete search space. The optimization problem that is solved

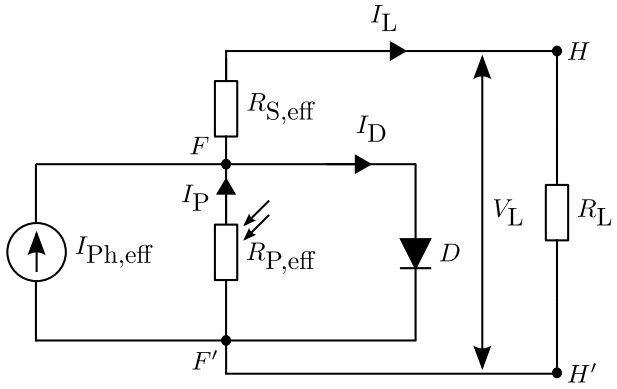

Fig. 2. Physical equivalent circuit of the solar panel to an effective single solar cell model [12].

can be expressed based on [49] as follows:

$$\min_{\substack{I_{0,eff},R_{S,eff},A_{eff}\\ R_{P,eff},I_{Ph,eff}}} \sum_{i=1}^{21}\Bigg| I_{0,eff}\Bigg\{ \exp\left\{\frac{q\left[V_L(i) - R_{S,eff}I_L(i)\right]}{A_{eff}k_B T}\right\} - 1\Bigg\} - \frac{V_L(i) - R_{S,eff}I_L(i)}{R_{P,eff}} - I_{Ph,eff} + I_L(i)\Bigg| \tag{36}$$

subject to :

$$I_{0,eff,min} \le I_{0,eff} \le I_{0,eff,max} \tag{37}$$
$$R_{S,eff,min} \le R_{S,eff} \le R_{S,eff,max} \tag{38}$$
$$A_{eff,min} \le A_{eff} \le A_{eff,max} \tag{39}$$
$$R_{P,eff,min} \le R_{P,eff} \le R_{P,eff,max} \tag{40}$$
$$I_{Ph,eff,min} \le I_{Ph,eff} \le I_{Ph,eff,max}. \tag{41}$$

Twenty one measurements are conducted for every V-P curve of the WPT systems implemented in Experiment I. The subscripts 'min' and 'max' of each of the five unknown parameters of (37)–(41) denote the real positive minimum and maximum value of the finite search space, respectively. The five identified parameters are first refined by the application of 'fsolve' in Matlab and the resulting values are applied to (33)–(35) for curve fitting of the experimental data. Note that the experimental measurements of I_L and V_L are also used for the determination of a local solution to this non-linear curve-fitting problem [50].

5) Total Link and Components Efficiency: An important aspect of the technology of WPT is the total efficiency of a link that is a function of the components efficiency. The external power efficiency of a LD can be defined as:

$$\eta_{LD} = \frac{P_{Tx,o}}{P_{in}} \times 100\%, \tag{42}$$

where P_{in} is the DC input electrical power to the optical source.

Line of sight (LoS) conditions are assumed for the optical wireless channel. So long as the experiments are conducted in an indoor environment, no atmospheric attenuation of the laser beam due to absorption from molecules and scattering effects (Mie or Rayleigh) with aerosol particles is considered [37],

[51]. Therefore, only geometrical losses of the transmitted optical power are assumed due to the laser beam divergence over distance.

In practice, the typical geometry of an optical receiver (solar cell or panel) is rectangular with an effective area of $S_{\text{eff}} = 2x_0 \times 2y_0$, where x_0 is the half length and y_0 is the half width. The ratio of the optical power collected by the rectangular solar receiver, $P_{\text{Rx,o}}(z)$, at a distance of $z \geq d_0 + t_{\text{c}}$ over the total transmitted optical power can be defined as the collection efficiency, $\eta_{\text{c}}(z)$. This factor can be calculated in the case of a single optical link by:

$$\eta_{\text{c}}(z) = \frac{P_{\text{Rx,o}}(z)}{(1-r)P_{\text{Tx,o}}} \times 100\% = \text{erf}\left[\frac{\sqrt{2}x_0}{W'_{\text{x}}(z')}\right]\text{erf}\left[\frac{\sqrt{2}y_0}{W'_{\text{y}}(z'')}\right] \times 100\%, \quad (43)$$

where $\text{erf}\,[.]$ denotes the error function. Quantities $W'_{\text{x}}(z')$ and $W'_{\text{y}}(z'')$ are given by (30) and (31), respectively. An analytical derivation of (43) is provided in Appendix B. This very useful parameter provides information about the geometrical losses of the optical link. In fact, the geometrical losses are determined by the efficiency of collimation of the optical source. As the beam divergence decreases, the geometrical losses decrease, accordingly, for a solar panel of constant dimensions. Therefore, the laser beam can propagate more efficiently at longer distances.

The most important metric of the energy efficiency of a solar panel or cell is the optical-to-electrical conversion efficiency. This factor is computed by [27]:

$$\eta_{\text{sr}}(z) = \frac{P_{\text{m}}}{P_{\text{Rx,o}}(z)} \times 100\%, \quad (44)$$

where P_{m} denotes the maximum electrical power and is given by $P_{\text{m}} = V_{\text{m}}I_{\text{m}}$. Also, V_{m} and I_{m} represent the voltage and current at the maximum power point (MPP) of the panel, respectively. The fill factor (FF) of a solar panel shows how well the circuit approximates the ideal behavior of a current source. The FF of a PV panel is given by [27]:

$$f_{\text{sr}} = \frac{V_{\text{m}}I_{\text{m}}}{V_{\text{oc}}I_{\text{sc}}} \times 100\%, \quad (45)$$

where V_{oc} and I_{sc} denote the open-circuit voltage and short-circuit current, respectively. The responsivity of the solar receiver can be defined as:

$$\rho(z) = \frac{I_{\text{Ph,eff}}}{P_{\text{Rx,o}}(z)}. \quad (46)$$

However, a common assumption of $I_{\text{Ph,eff}} \simeq I_{\text{sc}}$ is made practically [52]. This is explained by the low series resistance and high parallel resistance of the solar panel. In this case, the responsivity becomes a purely measurable quantity as both the short-circuit current and the received optical power can be measured.

Finally, the maximum link efficiency is computed by:

$$\eta_{\text{max}} = \frac{P_{\text{m}}}{P_{\text{in}}} \times 100\%. \quad (47)$$

TABLE II
ANALYTICAL PARAMETERS FOR THE DETERMINATION OF d_{NOHD}

Parameter	Unit	Value	Parameter	Unit	Value
λ_0	[nm]	660.00	A	-	0.836
$P_{\text{Tx,o,m}}$	[mW]	130.00	B	[mm]	4.93
$W_{0\text{x}}$	[μm]	1.92	C	[cm^{-1}]	−1.247
$W_{0\text{y}}$	[μm]	1.12	D	-	0.46
x_0	[mm]	3.50	$R_{2\text{x}}$	[cm]	13.93
d_0	[mm]	3.25	$R_{2\text{y}}$	[cm]	13.93
$W_{1\text{x}}$	[μm]	355.62	$W_{2\text{x}}$	[μm]	837.21
$W_{1\text{y}}$	[μm]	609.62	$W_{2\text{y}}$	[mm]	1.44
$R_{1\text{x}}$	[mm]	3.25	$d_{1\text{x}}$	[cm]	−13.91
$R_{1\text{y}}$	[mm]	3.25	$d_{1\text{y}}$	[cm]	−13.93

The combination of (42)–(47) forms an expression of the maximum link efficiency as a function of the LD, lens, collection and solar receiver efficiency given by:

$$\eta_{\text{max}} = \eta_{\text{LD}}(1-r)\eta_{\text{c}}(z)\eta_{\text{sr}}(z) \times 100\% = \eta_{\text{LD}}(1-r)\eta_{\text{c}}(z)f_{\text{sr}}\rho(z)V_{\text{oc}} \times 100\%, \quad (48)$$

where the assumption of $I_{\text{Ph,eff}} \simeq I_{\text{sc}}$ is made.

C. Eye Safety Regulations

Important parameters for eye safety are given below for the LD used in all of the experiments and the LD and collimation lens used in Scenario II of Experiment I according to the British Standard BS EN 60825-1:2014 [11]. The classification process is shown analytically in Appendices C and D.

1) Single Laser Diode: The LD used in the experiments (i.e. HL6544FM) has not been classified by the manufacturer [43]. For this reason, a methodology for its classification is presented in Appendix C, based on [11]. This methodology leads to the conclusion that the LD is classified as Class 3B. Laser products of Class 3B are normally hazardous when there is intrabeam ocular exposure, i.e. within the nominal ocular hazard distance (NOHD), d_{NOHD}, according to [11]. Also, the viewing of diffuse reflections is normally safe. The accessible emission limit (AEL), κ, of Class 3B is $\kappa = 500\,\text{mW}$ according to Table 8 of [11]. The maximum permissible exposure (MPE), ν, is determined from Table A.1 [11] to be $\nu = 10\,\text{W/m}^2 = 1\,\text{mW/cm}^2$. The LD irradiance measured from a square aperture stop with side length $2x_0$ at a distance z is computed by:

$$G_{\text{Rx}}(z) = \frac{\text{erf}\left[\frac{\sqrt{2}x_0}{W_{\text{x}}(z)}\right]\text{erf}\left[\frac{\sqrt{2}x_0}{W_{\text{y}}(z)}\right]P_{\text{Tx,o,m}}}{(2x_0)^2}, \quad (49)$$

where $P_{\text{Tx,o,m}}$ denotes the maximum output optical power of the LD; and $W_{\text{x}}(z)$ and $W_{\text{y}}(z)$ are given by (3) and (4), respectively. In order to determine the NOHD, the inequality $G_{\text{Rx}}(d_{\text{NOHD}}) \leq \nu = 1\,\text{mW/cm}^2$ needs to be solved. The graphical solution of this inequality, i.e. the intersection point of the two curves representing $G_{\text{Rx}}(z)$ and ν, for the applied values of λ_0 to x_0 given in Table II, to (3), (4) and (49) results in $d_{\text{NOHD}} = 63\,\text{cm}$. Therefore, a safe setup requires proper enclosure of the beam inside a tube with a length of 63 cm from the LD. This is because visual access to the laser beam and its specular reflections inside the NOHD must be prevented.

TABLE III
STUDY I: DATA SHEET PARAMETERS OF COMPONENTS

Laser diode			Aspheric lens			Multi-crystalline silicon solar panel			Mono-crystalline silicon solar cell		
Parameter	Unit	Value	Parameter	Unit	Value	Parameter	Unit	Value	Parameter	Unit	Value
λ_0	[nm]	660.0	Δ	[cm]	1.27	N_c	-	8	N_c	-	1
$\vartheta_{\parallel}$	[mrad]	174.5*	R_1	[mm]	15.65	S_{eff}	[cm^2]	68.64	S_{eff}	[cm^2]	156.25
	[deg]	10.0*	R_2	[mm]	−4.75	P_m	[W]	0.80†	P_m	[W]	2.91†
$\vartheta_{\perp}$	[mrad]	296.7*	t_c	[mm]	7.50	η_{sr}	(%)	11.66†	η_{sr}	(%)	18.62†
	[deg]	17.0*	f	[mm]	8.02	f_{sr}	(%)	72.46†	f_{sr}	(%)	78.53†
$P_{Tx,o}$	[mW]	50.0**	n	-	1.52						
η_{LD}	(%)	22.2**	r	(%)	0.25						

*Full width at half maximum (FWHM) values, **typical values and †standard test conditions (STC) values [53]

2) Laser Diode and Collimation Lens: When the optical beam of a LD is collimated by the use of a lens, its optical and geometrical characteristics are modified compared with the use case of a single LD. Therefore, reclassification of the laser is required. This process is analyzed in Appendix D. Even in this case, the laser system is classified as Class 3B. Again, the AEL is 500 mW. However, the MPE is given in Table A.2 of [11] by $\nu = 18C_6T_2^{-0.25}$ [W/m^2] for $t > T_2$, where C_6 is a correction factor computed in Appendix D to be 10.867. Parameter T_2 is determined from Table 9 of [11] to be $T_2 = 10\times10^{[(\alpha-\alpha_{min})/98.5]} = 10\times10^{[(16.3-1.5)/98.5]} = 14.13$ s, where α and α_{min} are defined and determined in Appendices C and D. Therefore, the value of MPE is calculated to be $\nu = 18 \times 10.867 \times 14.13^{-0.25} = 100.89$ W/m^2 $= 10.09$ mW/cm^2. Here, the irradiance of the optical transmitter measured from a square aperture stop with side length $2x_0$ at a distance z is given by:

$$G'_{Rx}(z) = \frac{\mathrm{erf}\left[\frac{\sqrt{2}x_0}{W'_x(z')}\right]\mathrm{erf}\left[\frac{\sqrt{2}x_0}{W'_y(z'')}\right]P_{Tx,o,m}}{(2x_0)^2}, \qquad (50)$$

where the assumption of $(1 - r) \simeq 1$ is made and $W'_x(z')$ and $W'_y(z'')$ are given by (30) and (31), respectively. Again, the inequality $G'_{Rx}(d_{NOHD}) \leq \nu = 10.09$ mW/cm^2 needs to be solved for the determination of d_{NOHD}. This inequality is solved graphically by the application of the values of Table II to (1)–(10), (14)–(31) and, finally, (50). The resulting value of NOHD is $d_{NOHD} = 3.6$ m and this means that the laser beam must be enclosed into a shielding tube of length of 3.6 m from the output surface of the lens for eye safety. For a safer practical setup with a smaller NOHD, either the distance between the LD and the lens should be modified so that the beam becomes more divergent inducing more geometrical losses to the link, or the transmission power should decrease according to the MPE level.

D. Experimental System and Results

The selected components, objectives, methods, setups, applied analytical models and results of Experiments I–III are given below.

1) System Components: The values of components' parameters from their respective data sheets [43], [54]–[56] are summarized in Table III. A single mode Opnext HL6544FM high power LD with a MQW structure is used as an optical source for power transmission [43]. This laser is a continuous wave (CW) source. The semiconductor material of this LD is aluminium gallium indium phosphide (AlGaInP). Angles $\vartheta_{\parallel}$ and $\vartheta_{\perp}$ refer to the full width at half maximum (FWHM) intensity along the parallel and perpendicular plane to the junction, respectively. The selected wavelength of 660 nm favors a visible and, therefore, uncomplicated alignment of the components. Also, the spectral responsivity of silicon (Si)-based receivers has large values in the red region of the VL spectrum [57]. The long wavelength of 1550 nm, widely used in FSO communications [37], is not considered because of the respective very low spectral responsivity of typical Si cells or panels [27].

The relatively large angular divergence of the optical source along both transverse x- and y- axes requires the use of a precise lens for light collimation. Lenses with spherical surfaces are low cost and are relatively uncomplicated to manufacture, but they have spherical aberrations [48]. In contrast, the complex geometry of aspheres allows for correction of spherical aberration and creates collimated beams of better quality [48]. In this study, an ACL12708U-A aspheric lens made of B270 optical crown glass with anti-reflection coating (ARC) is used in Experiments I and III [54].

The off-the-shelf optical receivers used for PH are a multi-c-Si solar panel and a mono-c-Si solar cell. In general, mono-c-Si cells have larger efficiency and are more expensive than multi-c-Si-based cells. More specifically, a MC-SP0.8-NF-GCS multi-c-Si-based panel with 8 cells connected in series is used in Scenario I of Experiment I [55]. The dimensions of this panel are 8.8×7.8 cm^2. Also, the mono-c-Si cell has dimensions of 12.5×12.5 cm^2 and is used in Scenario II of Experiment I [56].

2) Experiment I – Objective, Method, Setup and Applied Analytical Model: The objective of Study I, to increase the experimental energy efficiency of the 5 m OW link created in [8] and [9], is undertaken in this experiment. The system block diagram created for WPT is shown in Fig. 3. The term 'optical transmitter' is defined as a single pair of a LD and an aspheric lens. First, an amount of electrical power, P_{in}, is supplied to a number, N_{Tx}, of optical transmitters. The LDs are connected in parallel. The optical power generated from either a single LD or multiple LDs, $P_{Tx,o}$, is passed through a single lens or multiple lenses for beam collimation. The distance between each LD and the respective input lens surface is adjusted so that the product of V_{oc} and I_{sc} is maximized at the solar receiver. The output optical power of a single lens or multiple lenses, $(1-r)P_{Tx,o}$, is transmitted through an indoor LoS wireless channel that induces mostly geometrical

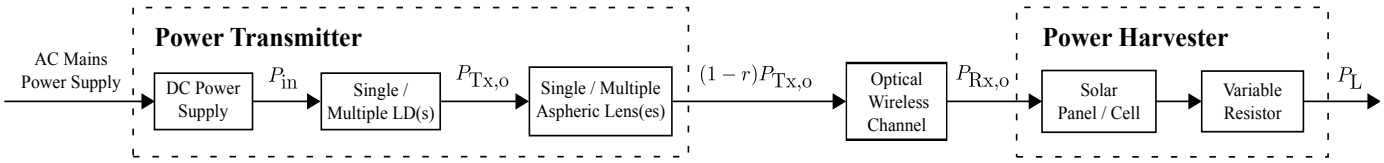

Fig. 3. System block diagram in Experiment I.

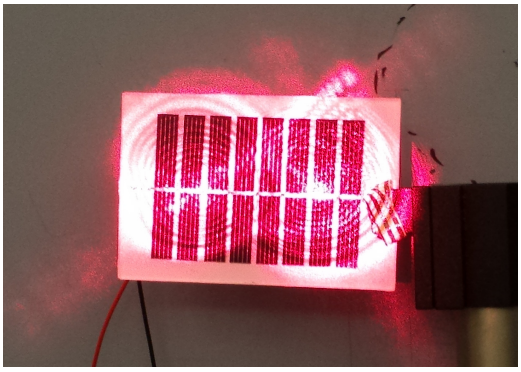

Fig. 4. Scenario I: Beam pattern formed by two optical transmitters on the solar panel.

Fig. 5. Scenario II: Beam pattern of three laser sources and measurement of P_{m}.

and misalignment losses. The optical power collected from the solar receiver (panel or cell) is $P_{\text{Rx,o}}$. A final amount of electrical power, P_{L}, is harvested from a variable resistor that represents the load of the PV panel or cell.

In Experiment I, the parameters of f_{sr}, η_{max} and P_{m} are determined. For this reason, the variable resistor is modified for the measurement of 21 pairs of $(V_{\text{L}}, I_{\text{L}})$ by the use of two multimeters. Also, the respective values of R_{L} are measured. The values of V_{L} and I_{L} are in the range $[0, V_{\text{oc}}]$ and $[0, I_{\text{sc}}]$, respectively. The link distance measured from the output surface of the lens to the input plane of the receiver is $5.2\,\text{m}$. The experimental data are fit by the application of (33)–(41) of the solar receiver physical model.

This experiment includes two different scenarios. In Scenario I, the number of N_{Tx} scales from 1 to 4, and the multi-c-Si panel is used. In Fig. 4, the pattern of two optical transmitters on the PV panel is illustrated. In Scenario II, the number of N_{Tx} increases from 1 to 3, and the mono-c-Si cell is used. In Fig. 5, the laser beam pattern on the solar cell for $N_{\text{Tx}} = 3$ and the measured voltage and current of the load are shown.

The experimental measurements of P_{L} over V_{L} for Scenarios I and II are shown in Fig. 6(a) and 6(b), respectively. The curves labeled as 'Physical Model' are generated by a local solution of (36). The measured parameters are presented in Table IV and the respective parameters of [8] and [9] are given for comparison reasons. Also, the five estimated parameters of the model of solar receiver are given in Table V.

Note that a peak harvested power is observed for each V-P curve in Scenarios I and II of Fig. 6. The peak electrical power harvested from a solar receiver is feasible under the conditions of perfect load matching. In this case, the characteristic resistance of the solar receiver (i.e. the output resistance at the MPP) is equal to the resistance of the load [58]. Thus, the maximum possible amount of electrical power is transferred to the load connected to the output of the solar cell or panel.

3) Scenario I – Results and Discussion: In Scenario I, the values of f_{sr}, η_{max} and P_{m} are quite low when one optical transmitter is used. In this case, the laser beam illuminates the whole rectangular area of the solar panel. Cells placed at the edges of the panel receive less optical power compared with the centrally placed ones due to the elliptical and Gaussian beam profile. Therefore, power generated by cells with higher received irradiance levels is dissipated by cells with lower irradiance levels. This effect induces mismatch losses among different cells of the panel. As a result, the total electrical output of the PV panel is determined by cells with the lowest performance.

A significant increase in the values of f_{sr}, η_{max} and P_{m} by at least 1.5, 2.9 and 5.6 times, respectively, is observed when $N_{\text{Tx}} > 1$ compared with the case of $N_{\text{Tx}} = 1$. When the number of optical transmitters is larger than 1, the laser beams cover smaller circular and elliptical areas mainly inside the panel area illuminating different cells as shown in Fig. 4 for $N_{\text{Tx}} = 2$. Thus, a more uniformly illuminated pattern is formed and the effect of mismatch losses becomes less significant. As N_{Tx} increases from 2 to 4, the values of f_{sr}, η_{max} and P_{m} increase gently, as expected due to the respective increase in $P_{\text{Rx,o}}$ and, therefore, η_{sr}. The multi-c-Si solar panel presents a significantly large f_{sr} value of 69% in the case of $N_{\text{Tx}} = 4$. Therefore, this receiver has a very high energy efficiency, very close to its STC value of 72.46%.

The values of f_{sr}, η_{max} and P_{m} for $N_{\text{Tx}} = 4$ are increased by the multiplication factors of 2, 26.6 and 1.7, respectively, compared with the values of the same parameters in our first experimental study [8]. This significantly improved performance, especially for η_{max}, is attributed to the large restriction of geometrical losses by the use of the more directive optical sources of LDs compared with LEDs, and to the higher energy

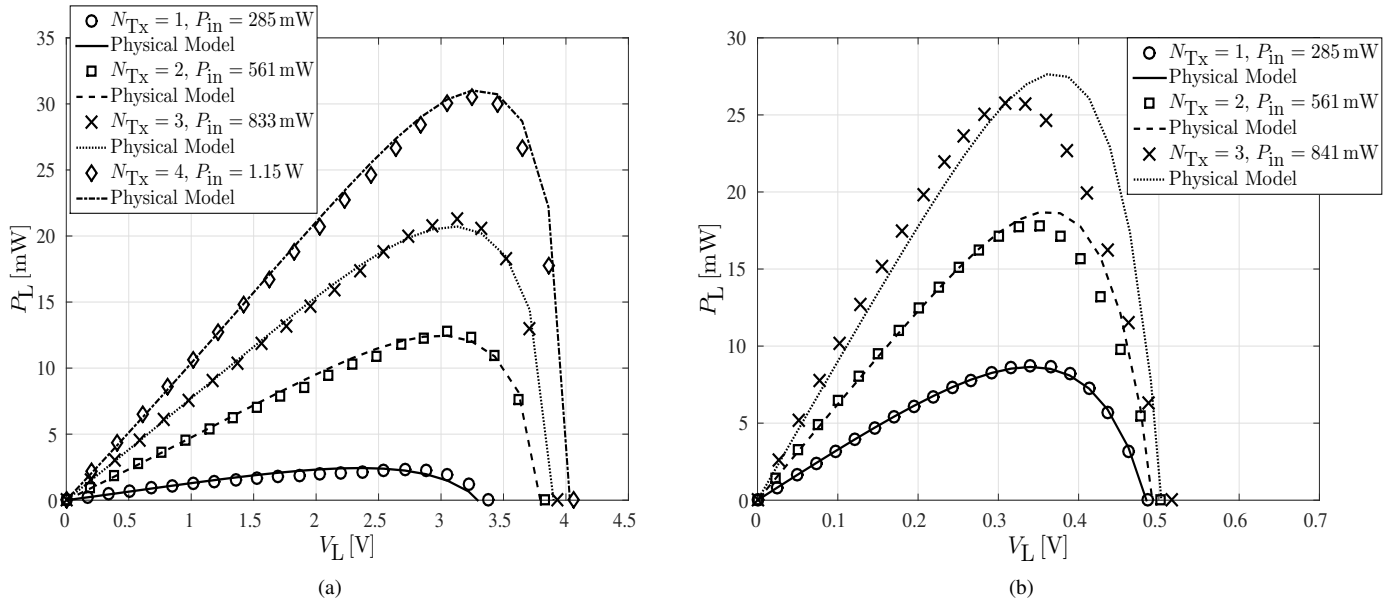

Fig. 6. Experiment I: Measured data of harvested electrical power versus load voltage of (a) Scenario I and (b) Scenario II supported by the physical model curves.

TABLE IV
MEASURED PARAMETERS OF EXPERIMENT I AND AUTHORS' PREVIOUS RESEARCH

Scenario I						Scenario II					
N_{Tx}	d_0 [mm]	f_{sr} (%)	$\eta_{\max}$ (%)	P_{m} [mW]	$R_{\mathrm{L}}^{\dagger}$ [Ω]	N_{Tx}	d_0 [mm]	f_{sr} (%)	$\eta_{\max}$ (%)	P_{m} [mW]	$R_{\mathrm{L}}^{\dagger}$ [Ω]
1	7.0*	45.08	0.80	2.3	3200	1	3.25**	53.35	3.06	8.7	13.5
2	6.0*	66.89	2.28	12.8	731	2	3.25***	54.20	3.17	17.8	7.3
3	5.5*	68.55	2.56	21.3	460	3		49.39	3.06	25.7	4.0
4	5.0*	69.03	2.66	30.6	344						
Measured Parameters in [8]						Measured Parameters in [9]					
N_{Tx}	d_0 [cm]	f_{sr} (%)	$\eta_{\max}$ (%)	P_{m} [mW]	$R_{\mathrm{L}}^{\dagger}$ [kΩ]	N_{Tx}	d_0 [mm]	f_{sr} (%)	$\eta_{\max}$ (%)	P_{m} [mW]	$R_{\mathrm{L}}^{\dagger}$ [kΩ]
1	16.8	31.12	0.08	7.69	1.43	1	3.8***	34.41	0.40	1.1	11.51
		30.20	0.10	18.32	2.07	2		34.69	0.52	2.9	8.45
						3		36.98	0.67	5.7	6.98
						4		39.27	0.63	7.3	5.57
						5		38.75	0.65	9.2	5.87
								36.20	0.74	10.4	4.56

Tolerance of * ± 0.5 mm, ** ± 0.75 mm and *** ± 0.25 mm.
†Measured at the maximum power point (MPP).

TABLE V
ESTIMATED PARAMETERS OF SOLAR RECEIVER MODEL FOR EXPERIMENT I

Scenario I						Scenario II					
N_{Tx}	$I_{0,\mathrm{eff}}$ [μA]	$R_{\mathrm{S,eff}}$ [Ω]	A_{eff}	$R_{\mathrm{P,eff}}$ [kΩ]	$I_{\mathrm{Ph,eff}}$ [mA]	N_{Tx}	$I_{0,\mathrm{eff}}$ [μA]	$R_{\mathrm{S,eff}}$ [Ω]	A_{eff}	$R_{\mathrm{P,eff}}$ [kΩ]	$I_{\mathrm{Ph,eff}}$ [mA]
1	312.83	500	65	5.0	1.3	1	675.57	1.04	4.82	26.3	33.3
2	54.69	110	32	4.0	4.7	2	107.89	0.08	3.02	27.0	62.6
3	52.96	70	30	4.5	7.7	3	144.29	0.03	3.05	90.0	90.5
4	21.85	50	25	3.0	10.2						

efficiency of multi-c-Si than that of a-Si technology of solar panels. Also, f_{sr}, $\eta_{\max}$ and P_{m} for $N_{\mathrm{Tx}} = 4$ are increased by the factors of 1.8, 4.2 and 4.2, respectively, compared with the same parameters obtained in [9]. These improved values are obtained due to the decrease in dimensions and number of cells of the solar panel that allows for the concentration of more optical power uniformly distributed on the cells. Thus, the effect of mismatch losses is less significant than that in [9].

The resistance load values measured at the MPP decrease from $3.2\,\mathrm{k\Omega}$ to $344\,\Omega$, while the received optical power increases. For a practical R_{L} value of $50\,\Omega$, better load matching can be achieved either by an increase in N_{Tx} and therefore $P_{\mathrm{Rx,o}}$, or by the use of a DC-to-DC converter for maximum power point tracking (MPPT) [59].

4) Scenario II – Results and Discussion: In Scenario II, the values of f_{sr} and $\eta_{\max}$ are expected to increase as the number of optical transmitters increases. However, this expectation is not confirmed in the case of $N_{\mathrm{Tx}} = 3$. This is explained by the significantly low decrease in effective series resistance value from $80\,\mathrm{m\Omega}$ ($N_{\mathrm{Tx}} = 2$) to $30\,\mathrm{m\Omega}$ ($N_{\mathrm{Tx}} = 3$) compared with the transition from $1.04\,\Omega$ ($N_{\mathrm{Tx}} = 1$) to $80\,\mathrm{m\Omega}$ ($N_{\mathrm{Tx}} = 2$),

as shown in Table V. Therefore, more power is dissipated in the series resistance and, finally, the fill factor and efficiency of the solar cell decrease. The series resistance of the cell decreases, when the incident optical power increases. This is attributed to the increase in the conductivity of the active layer [60]. Also, note that the curve of maximum link efficiency as a function of harvested power in Scenario II shown in Fig. 7 is in close agreement with the curve of solar cell efficiency versus incident optical power in [61].

Comparing the two scenarios, the best value of $\eta_{\max} = 3.17\%$ is achieved in the case of $N_{\text{Tx}} = 2$ for Scenario II. Note that this value of maximum link efficiency is low because of the low values of η_{LD} and $\eta_{\text{sr}}(5.2\,\text{m})$ as shown in Section III-D7.

A comparison of the values of f_{sr} and $\eta_{\max}$ for $N_{\text{Tx}} = 2$ with the values of the same parameters in [8] shows an increase of 1.6 and 32 times, respectively. The same comparison with the results of [9] presents an increase by 1.6 and 6.2 times, respectively. Also, quantity P_{m} for $N_{\text{Tx}} = 3$ is increased by the factors of 1.4 and 4.4 compared with [8] and [9], respectively. A slightly better performance in terms of $\eta_{\max}$ of Scenario II compared with Scenario I is observed. This is attributed to the larger optical-to-electrical conversion efficiency of mono-c-Si cell than that of multi-c-Si panel as expected by observing Table III. Also, the larger area of 2.3 times of the PV cell compared with the solar panel allows for the reception of a larger amount of $P_{\text{Rx,o}}$ reducing the geometrical losses.

Finally, the values of measured R_{L} at the MPP are quite low due to the low values of V_{L}. Therefore, matching of the output of the cell with a practical load of $50\,\Omega$ can be achieved either by a DC-to-DC converter or by the connection of a large number of cells in series.

5) Comparison of Scenarios I and II with an Inductive Power Transfer System: In [10], a state-of-the-art experimental study is presented by the implementation of an IPTS with dipole coils able to deliver amounts of power in the order of hundreds of W. In Fig. 16 of [10], the power efficiency measured from the input of the inverter to the load resistor is plotted as a function of the power harvested from the load for different values of distance of 2 m, 3 m, 4 m and 5 m. The operating frequency of the system is 105 kHz [10]. A comparison of the OW systems implemented in the two Scenarios of Experiment I and the IPTS is shown in Fig. 7 in terms of link efficiency at a distance of 5 m. When Scenario II is applied, the maximum link efficiency is improved from a value of 1.17% to 3.17% that represents a significant increase of 2.7 times. Therefore, taking into account the fact that IPTSs are designed to operate at short distances of a few cm [14] or m [10], the developed double OW link has an acceptable value of $\eta_{\max}$ and the link distance can be further extended.

6) Experiment II – Objective, Method, Setup, Applied Analytical Model and Results: The objective of Experiment II is to determine the efficiency values of each of the 4 LDs as a function of their input power. Therefore, the output optical power of each LD is measured for 22 different values of input electrical power. A Thorlabs S121B Si sensor with a square area of $1 \times 1\,\text{cm}^2$ is placed at 1.5 mm from each LD in order to collect and measure the total amount of optical power of each laser beam. The mean values of experimental data are fit by two simple quadratic curves applied to the two operation regions of the device. These two regions are characterized by spontaneous and stimulated emission, respectively.

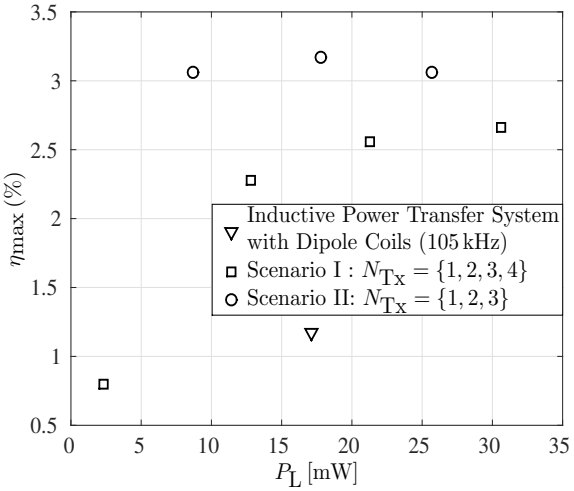

Fig. 7. Experimental maximum link efficiency versus the maximum harvested electrical power.

The external power efficiency of the 4 LDs is shown in Fig. 8 as a function of P_{in}. The maximum efficiency values of the 4 LDs shown as #1, #2, #3 and #4 are measured to be 28.1%, 30.2%, 32.2% and 32.9%, respectively. In the first region of the theoretical curve, the output optical power remains at very low levels of up to 94.6 μW, as P_{in} increases from 0 mW to 95.4 mW. Also, for the same values of P_{in}, the mean value of power efficiency of the 4 LDs ranges from 0.05% to 0.1%. This region of applied P_{in} causes spontaneous emission to the LD, one of the basic forms of interaction between atoms and photons in quantum physics [62]. In spontaneous emission, an atom transits from an upper energy level, E_2, to a lower energy level, E_1, releasing a photon, and this is a random process. In the second region of the theoretical curve, $P_{\text{Tx,o}}$ increases significantly up to 86.1 mW with a respective efficiency of 29.1%, while P_{in} scales from 95.4 mW to 320 mW. This region of P_{in} induces stimulated emission to the optical source [62]. In stimulated emission, a photon of energy $E_2 - E_1$ interacts with an atom placed at an upper energy level. This atom transits to a lower energy level emitting a second photon of similar characteristics with the first one.

In order to compare the variation between the 4 LDs, the error in efficiency, ϵ_{eff} (%), is used and is defined as the difference in theoretical efficiency by the experimental efficiency data for each LD. Fig. 9 shows how the error in efficiency of the 4 LDs scales with the input electrical power of each LD. The mean squared error (MSE) in power efficiency of each of the LDs is calculated to be $3.52 \cdot 10^{-4}$, $3.46 \cdot 10^{-4}$, $3.13 \cdot 10^{-5}$ and $4.89 \cdot 10^{-4}$. This means that the LD shown as #3 in Fig. 8 and Fig. 9 best approximates the efficiency values of the theoretical curve. In the case of a large number of LDs, such as the 42-based laser transmitter designed in Section V, the variation of LDs is expected to affect the harvested power. Therefore, to affirm 1 W with high confidence, the required number of optical sources should be estimated based on the

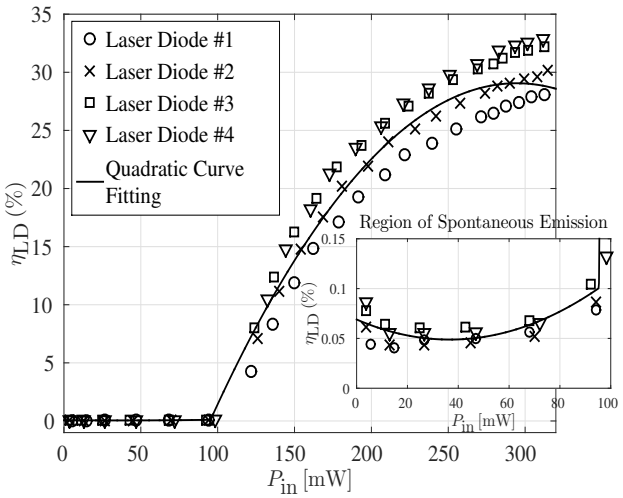

Fig. 8. Experiment II: Laser diodes efficiency versus input electrical power.

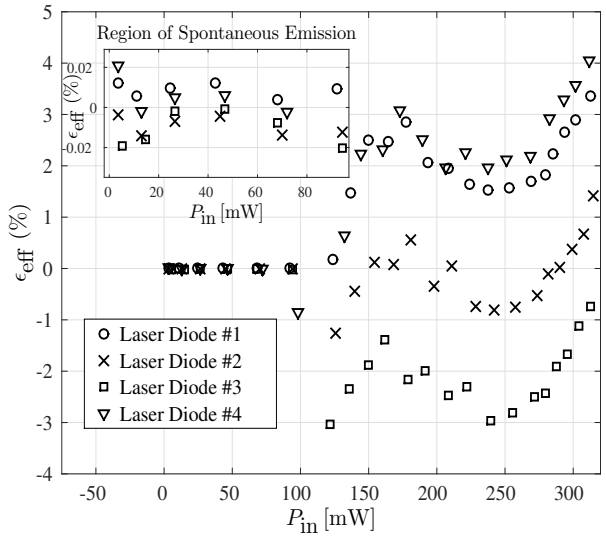

Fig. 9. Experiment II: Efficiency error as a function of input electrical power for 4 laser diodes.

LD with the lowest efficiency.

7) Experiment III – Objective, Method, Setup and Results: Experiment III is undertaken for the determination of the solar cell efficiency. Two LDs with aspheric lenses are transmitting power to the mono-c-Si cell placed at a distance of 5.2 m. The electrical input power is 561.3 mW. The S121B sensor is used for the measurement of 25 values of power, P_s, at a distance of 3.4 cm from the solar cell. The measurement points are located on a square grid as shown in Fig. 10. The distance between two consecutive points is 2.08 cm. The average irradiance of the 25 measured points is computed and is multiplied by S_{eff}. Therefore, the value of $P_{\text{Rx,o}}(5.2\,\text{m})$ is calculated, and the parameters of $\eta_{\text{sr}}(5.2\,\text{m})$, $\rho(5.2\,\text{m})$ and $\eta_{\text{c}}(5.2\,\text{m})$ are determined from (44), (46) and (48), respectively.

The 25 measured data of P_s are shown in Fig. 11 versus the x- and y-dimensions of the solar cell. The power of each of the two optical transmitters measured at the (x, y, z) points of $(0, 0, 3.7\,\text{cm})$ and $(0, 0, 3.2\,\text{cm})$ is 74.58 mW and 72.8 mW, respectively. These values are significantly attenuated at a distance of 5.2 m from the transmitters. In particular, the maximum optical power measured at the (x, y, z) point of $(0, 2.08\,\text{cm}, 5.2\,\text{m})$ is 3.12 mW. The average irradiance value of these 25 measurements is $0.86\,\text{mW}/(1\,\text{cm}^2) = 0.86\,\text{mW/cm}^2$. Therefore, the received optical power of the cell is calculated to be $P_{\text{Rx,o}}(5.2\,\text{m}) = 0.86 \times 12.5^2 = 134.38\,\text{mW}$.

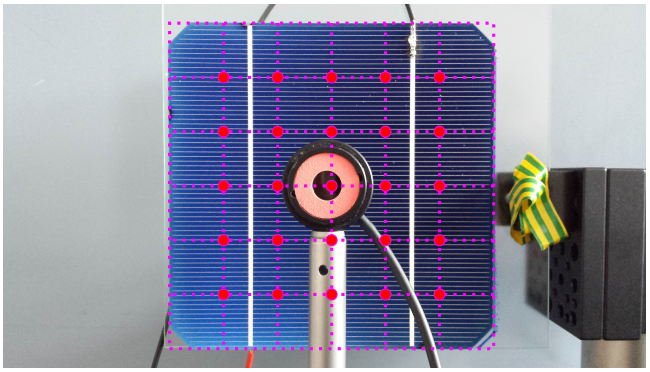

Fig. 10. Experiment III: Measurement points of irradiance for the calculation of $P_{\text{Rx,o}}$ in front of the solar cell.

The application of $P_{\text{m}} = 17.8\,\text{mW}$ and $P_{\text{Rx,o}} = 134.38\,\text{mW}$ to (44) results in $\eta_{\text{sr}}(5.2\,\text{m}) = 13.25\%$ in the case of $N_{\text{Tx}} = 2$. This value of solar receiver efficiency is 5.37% lower than the respective one at STC (see Table III) and therefore the cell is able to accommodate more optical power. For this reason, the specific mono-c-Si cell is selected to be the receiver in the simulation model developed for the objective of harvesting 1 W in Study III. Moreover, the maximum power that this cell can generate under STC is 2.91 W according to Table III that is larger than the required amount of 1 W.

So long as the experimental value of $\eta_{\text{sr}}(5.2\,\text{m})$ is now known, an estimation of the collection efficiency can be made using (48). The term $(1 - r)$ of (48) is assumed to be negligible because $r = 0.0025 \ll 1$. The input electrical power of 561 mW is equally supplied to the two optical transmitters. Thus, the electrical-to-optical efficiency of two optical transmitters for $P_{\text{in}} = 561\,\text{mW}$ is the same as η_{LD} of $N_{\text{Tx}} = 1$ for $P_{\text{in}} = 280.5\,\text{mW}$. Also, a mean value of $\eta_{\text{LD}} = 26.76\%$ is calculated for $P_{\text{in}} = 280.5\,\text{mW}$ based on the quadratic curve fitting of Fig. 8. Therefore, the application of $\eta_{\text{max}} = 0.0317$, $\eta_{\text{LD}} = 0.2676$ and $\eta_{\text{sr}}(5.2\,\text{m}) = 0.1325$ to (48) results in the collection efficiency value of $\eta_{\text{c}}(5.2\,\text{m}) = 89.4\%$. This very high value allows for the characterization of the link with 2 LDs as highly directive so that it effectively delivers 134.38 mW to a solar cell area of $12.5 \times 12.5\,\text{cm}^2$ placed at 5.2 m with only 10.6% of optical losses.

Finally, the application of $I_{\text{Ph,eff}} = 62.6\,\text{mA}$ and $P_{\text{Rx,o}}(5.2\,\text{m}) = 134.38\,\text{mW}$ to (46) gives an estimated responsivity of $\rho(5.2\,\text{m}) = 0.47\,\text{mA/mW}$. An experimental value of responsivity of $\rho(5.2\,\text{m}) = 0.49\,\text{mA/mW}$ is obtained under the assumption of $I_{\text{Ph,eff}} \simeq I_{\text{sc}} = 65.4\,\text{mA}$.

8) Estimation of the Number of Optical Transmitters: Let $N_{\text{Tx,req}}$ be the required number of pairs of LDs and lenses for harvesting 1 W at a 5.2 m link distance. In Scenario II of Experiment I, a value of $V_{\text{m}} = 351\,\text{mV}$ is achieved with $P_{\text{m}} =$

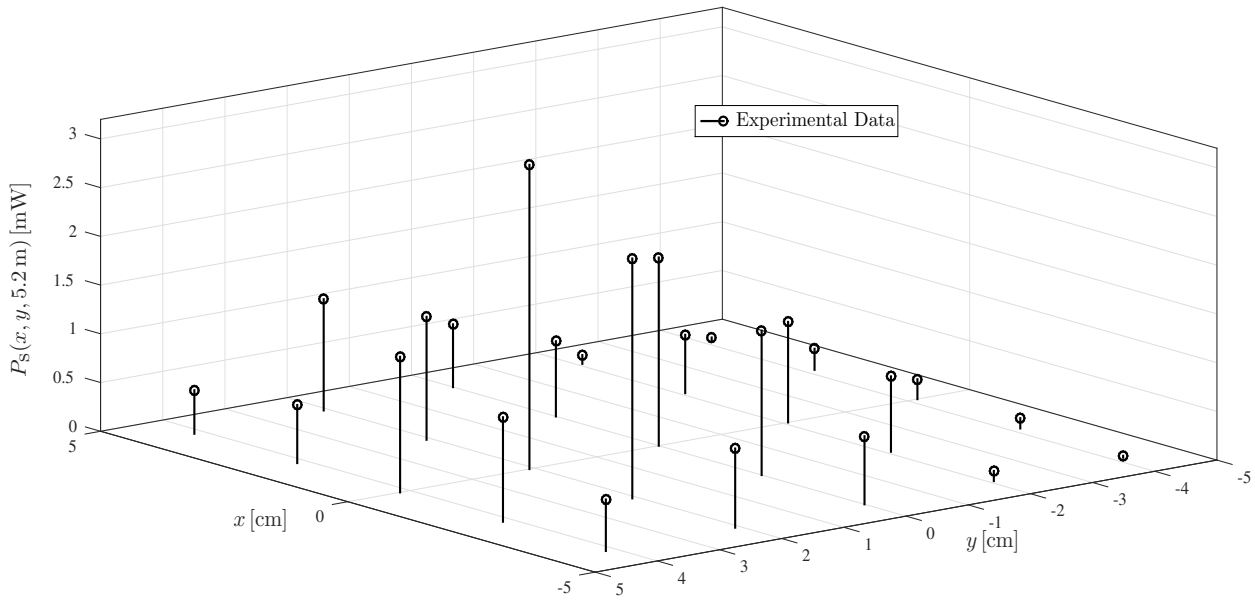

Fig. 11. Experiment III: Optical power measured by a sensor on the x-y transverse plane of the solar cell.

17.8 mW for $N_{\mathrm{Tx}} = 2$. Therefore, a required voltage $V'_{\mathrm{m}} = 537\,\mathrm{mV}$ is assumed for the solar cell at high illumination levels for attaining $P'_{\mathrm{m}} = 1\,\mathrm{W}$ according to [56]. The load current at MPP is calculated to be $I'_{\mathrm{m}} = 1/0.537 = 1.86\,\mathrm{A}$. The values of 537 mV and 1.86 A are substituted for V_{L} and I_{L}, respectively, in the 'exhaustive' search algorithm (36). This results in the following set of parameters: $(I_{0,\mathrm{eff}}, R_{\mathrm{S,eff}}, A_{\mathrm{eff}}, R_{\mathrm{P,eff}}, I_{\mathrm{Ph,eff}}) = (83.9\,\mathrm{pA},\ 0.5\,\mathrm{m\Omega},\ 1,\ 500\,\mathrm{k\Omega},\ 1.96\,\mathrm{A})$. The responsivity of the solar panel is considered to be $\rho = 0.49\,\mathrm{A/W}$, as measured in Experiment III. Solving (46) for $P_{\mathrm{Rx,o}}$ results in: $P_{\mathrm{Rx,o}} = I_{\mathrm{Ph,eff}}/\rho = 1.96/0.49 = 4\,\mathrm{W}$. An assumption of 10.6% of geometrical optical losses is made, as measured in Experiment III. Thus, the transmitted optical power is calculated to be $P_{\mathrm{Tx,o}} = P_{\mathrm{Rx,o}}/\eta_{\mathrm{c}} = 4/0.894 = 4.47\,\mathrm{W}$. Therefore, the required number of optical transmitters is calculated to be: $N_{\mathrm{Tx,req}} = 4.47/(73.69 \times 10^{-3}) \approx 61$, where 73.69 mW is the average output optical power of the 2 LDs measured in Experiment III.

9) Variation of Harvested Power and Link Efficiency Induced by the Application of Data Communication: In order to investigate the variation of PH and link efficiency induced by the reception of an information signal, an experiment with the solar receiver designed in [35] is undertaken. In particular, a single optical transmitter transfers power and data simultaneously to the solar panel placed at a link distance of 5.2 m. Also, an orthogonal frequency division multiplexing (OFDM) signal with adaptive bit and energy loading is applied for communication [35]. The OFDM signal has a single sided communication bandwidth of 5 MHz. An average data rate of 16.6 Mb/s is achieved at the receiver with a respective average bit error rate (BER) of $1.52 \cdot 10^{-3}$. Fig. 12 shows how the harvested power of the load scales with voltage, with and without the reception of the alternating current (AC) communication signal. A 4^{th} degree polynomial is applied to the experimental data for curve fitting. The harvested power of the load remains the same, even when an OFDM signal is received. So long as the time domain OFDM signal has a zero mean value, the DC biased optical OFDM signal has the mean value of the DC bias. The receiver circuit comprises one branch for EH and a second branch for data communication with an inductor and a capacitor, respectively. Therefore, the EH branch captures the DC component, whereas the communication branch captures the AC signal. Finally, since the input electrical power to the transmitter is constant, the link efficiency also remains unaffected by the communication signal received.

IV. Study II: Laser Beam Collimation

The objective, method, setup, applied analytical model and results of Experiment IV of Study II are summarized in Table VI.

A. Objective

The objective of Study II is the creation of an OW link able to transmit power efficiently at long distances, such as $100\,\mathrm{m} - 300\,\mathrm{m}$. Thus, Experiment IV is undertaken for the determination of beam divergence with a targeted value of 1 mrad. For this reason, the collimation capability of a large diameter lens is investigated. The motivation of using a relatively large optical element in front of the LD is two-fold. Firstly, the etendue law, also known as brightness theorem, states that the product of source area and the solid angle subtended by the system's entrance pupil as seen by the source remains constant in an optical system with passive components [63], [64]. This means that decreased beam divergence and, therefore, efficient

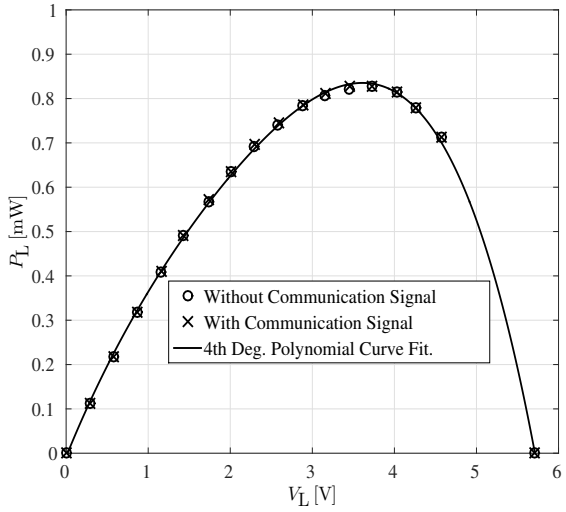

Fig. 12. V-P curve of resistor load with and without the application of a communication signal.

TABLE VI
SUMMARY OF EXPERIMENT IN STUDY II

Study II		Laser beam collimation	
Experiment		IV	
Objective		Determination of beam divergence with a target of 1 mrad	
Method		Measurement of diameter of circular laser beam images and 23 values of received optical power	
Setup			
	Optical source	Single laser diode	
	Optics	Spherical lens	
	Receiver	Optical power sensor	
	Measurement device	Optical power sensor	
	Link distance	4 m and 8 m	
Analytical model		(1)–(10) and (14)–(32)	
Results		Definition I	Definition II
		$\psi = 2.1$ mrad	$\psi_x = 3$ mrad $\psi_y = 5.8$ mrad

beam collimation can be achieved by a respective increase in dimensions of the lens. Also, a lens with large diameter is able to spread the optical power received from the LD decreasing the irradiance values along any of its transverse planes. Therefore, eye safety is improved, and the product of LD-lens can be classified as a lower Class [11].

B. Experimental System and Results

1) Experiment IV – Method, Setup and Applied Analytical Model: The characteristics of the red LD used in this experiment are given in Table III. Also, a 45-368 plano-convex (PCX) spherical lens made of borosilicate glass Schott BK7 with magnesium fluoride (MgF_2) ARC is used [65]. The features of the lens are given in Table VII.

In Experiment IV, the beam generated from the LD is collimated by the PCX spherical lens placed at $d_0 = 5.15$ cm from the LD with a tolerance of ± 0.5 mm. The optical power emitted from the LD is measured to be 4.76 mW. The pattern of circular and elliptical image of the lens and LD, respectively, at 4 m from the output surface of the lens are shown in Fig. 13. The beam divergence is defined and determined in two different ways. First, the beam divergence is defined as the plane angle of the truncated cone created by the circular image that is measured at two different link distances, d_1 and d_2. In particular, the diameter of the circular image, D_{im}, is measured at $d_1 = 4$ m and $d_2 = 8$ m, respectively. In this case, the beam divergence is calculated by:

$$\psi = 2\tan^{-1}\left[\frac{D_{\text{im}}(d_2) - D_{\text{im}}(d_1)}{2(d_2 - d_1)}\right]. \tag{51}$$

Also, note that the new beam waist is located before the distance of 4 m so that the images at 4 m and 8 m belong entirely to a diverging cone.

So long as the first definition does not include any information of the beam intensity, a second definition is used. In particular, the half width of the beam is estimated at the two points where the irradiance is decreased by $1/e$ times or 36.8% of the peak irradiance. For this reason, appropriate curve fitting with the analytical model presented in Sections III-B1, III-B2 and III-B3 is applied to the data measured along the 'slow' x- and 'fast' y- axes, respectively. A number of 23 irradiance measurements is conducted at the distances of 4 m and 8 m inside the semi circle of the image. Also, the illumination symmetry around both axes enables the calculation of the received optical power inside the circular image. Here, the beam divergence along the x- and y- axis is calculated by:

$$\psi_x = 2\tan^{-1}\left[\frac{W'_x(d_2) - W'_x(d_1)}{d_2 - d_1}\right] \tag{52}$$

TABLE VII
STUDY II: DATA SHEET PARAMETERS OF LENS

Parameter	Δ	R_1	R_2	t_c	f	n	r
Unit	[cm]	[mm]	[mm]	[mm]	[cm]	-	(%)
Value	7.5	∞	-38.76	32.68	7.5	1.52	1.5

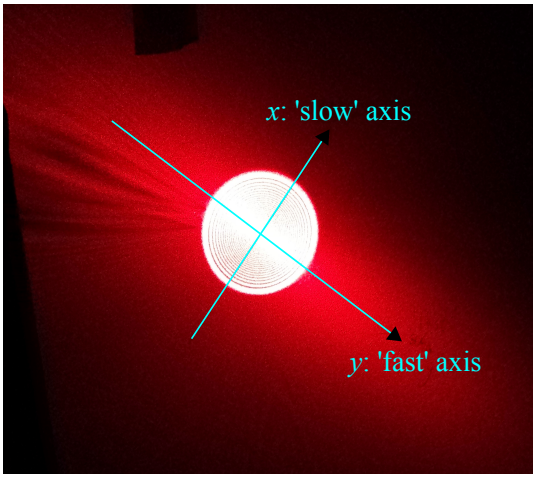

Fig. 13. Experiment IV: Beam pattern and vertical axes for the determination of beam divergence.

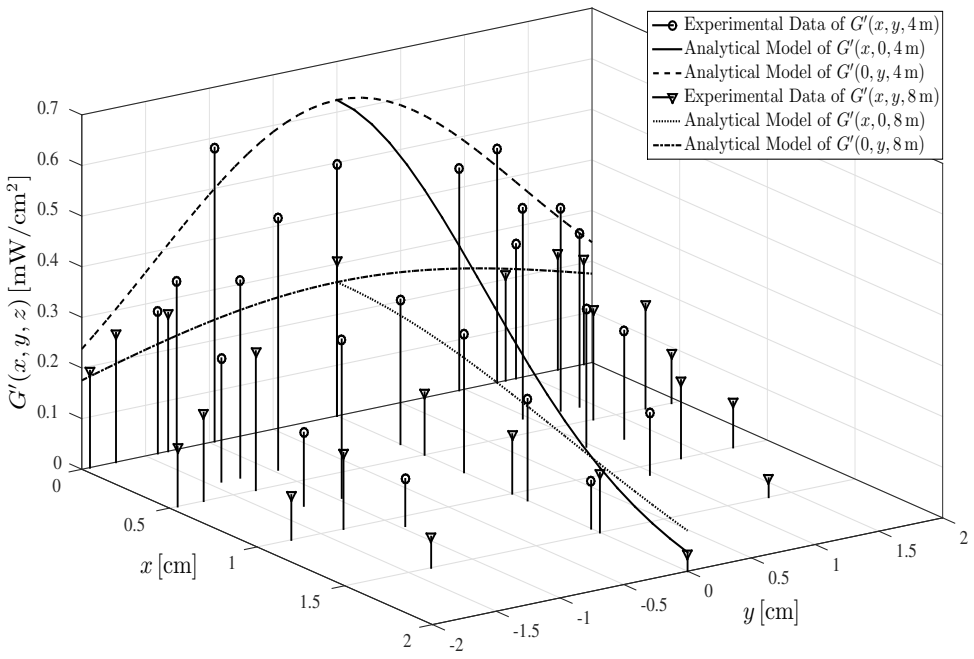

Fig. 14. Experiment IV: Data of irradiance on the x-y transverse plane of the laser beam at $4\,\mathrm{m}$ and $8\,\mathrm{m}$ accompanied by the respective analytical model curves.

TABLE VIII
ANALYTICAL PARAMETERS FOR CURVE FITTING OF DATA IN EXPERIMENT IV

Parameter	Unit	Value	Parameter	Unit	Value
$P_{\mathrm{Tx,o}}$	[mW]	4.76	A	-	1.00
λ_0	[nm]	660.00	B	[mm]	21.50
ϑ_{x}	[deg]	6.25	C	[m^{-1}]	-13.42
ϑ_{y}	[deg]	10.60	D	-	0.712
$W_{0\mathrm{x}}$	[µm]	1.92	$W_{2\mathrm{x}}$	[mm]	7.99
$W_{0\mathrm{y}}$	[µm]	1.12	$W_{2\mathrm{y}}$	[mm]	13.66
G_0	[kW/cm^2]	140.70	$R_{2\mathrm{x}}$	[m]	3.54
d_0	[cm]	5.15	$R_{2\mathrm{y}}$	[m]	3.54
$W_{1\mathrm{x}}$	[mm]	5.64	$d_{1\mathrm{x}}$	[m]	-3.54
$W_{1\mathrm{y}}$	[mm]	9.64	$d_{1\mathrm{y}}$	[m]	-3.54
$R_{1\mathrm{x}}$	[mm]	51.50	$W_{3\mathrm{x}}$	[µm]	92.93
$R_{1\mathrm{y}}$	[mm]	51.50	$W_{3\mathrm{y}}$	[µm]	54.39

and

$$\psi_{\mathrm{y}} = 2\tan^{-1}\left[\frac{W'_{\mathrm{y}}(d_2) - W'_{\mathrm{y}}(d_1)}{d_2 - d_1}\right], \tag{53}$$

respectively. The values of $W'_{\mathrm{x}}(z)$ and $W'_{\mathrm{y}}(z)$ denote the beam radii up to the $1/e$ points of peak irradiance along the x- and y-direction and have already been defined in (30) and (31), respectively.

2) Experiment IV – Results and Discussion: The diameters of the circular images at $4\,\mathrm{m}$ and $8\,\mathrm{m}$ are measured to be $2.9\,\mathrm{cm}$ and $3.75\,\mathrm{cm}$, respectively. Thus, the application of $d_1 = 4\,\mathrm{m}$, $d_2 = 8\,\mathrm{m}$, $D_{\mathrm{im}}(4\,\mathrm{m}) = 2.9\,\mathrm{cm}$ and $D_{\mathrm{im}}(8\,\mathrm{m}) = 3.75\,\mathrm{cm}$ to (51) results in a measured beam divergence of $\psi = 2.12\,\mathrm{mrad}$. This value is very close to the objective of $1\,\mathrm{mrad}$ that is achievable by the use of a lens with even larger diameter than that of the spherical one. Also, the optical power contained in the circular image is measured to be $1.94\,\mathrm{mW}$ and $1.87\,\mathrm{mW}$ at $d_1 = 4\,\mathrm{m}$ and $d_2 = 8\,\mathrm{m}$, respectively. Therefore, 40.8% and 39.3% of the transmitted optical power of $P_{\mathrm{Tx,o}} = 4.76\,\mathrm{mW}$ is included in the circular image at $4\,\mathrm{m}$ and $8\,\mathrm{m}$, respectively. This means that the lens placed at $5.15\,\mathrm{cm}$ from the LD fails to collect and collimate the whole optical power of the source inducing geometrical losses. Finally, the elliptical image (see Fig. 13) includes the remaining amount of optical power.

The experimental data of intensity at $4\,\mathrm{m}$ and $8\,\mathrm{m}$ fitted by the respective curves of analytical model are shown in Fig. 14. The curves labeled as 'Analytical Model' are derived by the use of (1)–(10) and (14)–(32). The analytical parameters used for curve fitting of the experimental data are shown in Table VIII. The slight deviation of some measured data points from the elliptical Gaussian fitting is explained by the existence of the diffraction effect [66]. This effect occurs when an optical wave passes through an aperture and is strongly dependent on the distance between the aperture and the observation plane, the wavelength and the aperture dimensions. In particular, here the diffraction effect stems from the transmission of the laser beam through the circular aperture of the lens mount to free space. The small black rings observed in the circular image of Fig. 13 and in Fig. 4 are translated to deep 'dips' of the irradiance. Also, even slight misalignment between the optical source and the lens can significantly affect the beam irradiance pattern observed at the far field. The application of the physical model of the elliptical Gaussian beam for curve fitting results in the values of $W'_{\mathrm{x}}(4\,\mathrm{m}) = 1.2\,\mathrm{cm}$ and $W'_{\mathrm{x}}(8\,\mathrm{m}) = 1.8\,\mathrm{cm}$. Therefore, the application of these values to (52) yields $\psi_{\mathrm{x}} = 3\,\mathrm{mrad}$.

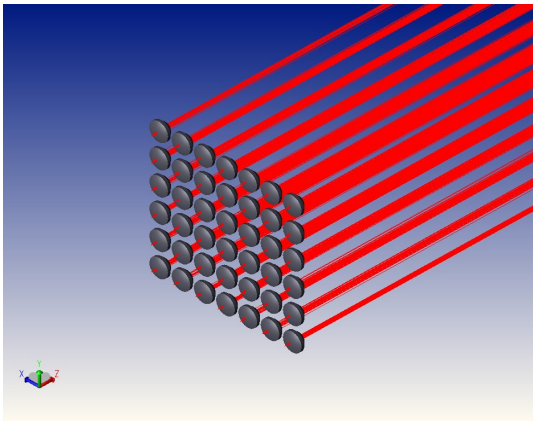

Fig. 15. Non-sequential components shaded model of the array of 7×6 laser diodes and lenses.

Similarly, the beam radius along the y-axis is calculated to be $W'_{\mathrm{y}}(4\,\mathrm{m}) = 2\,\mathrm{cm}$ and $W'_{\mathrm{y}}(8\,\mathrm{m}) = 3.15\,\mathrm{cm}$. Therefore, the beam divergence of the 'fast' axis is computed to be $\psi_{\mathrm{y}} = 5.75\,\mathrm{mrad}$ by (53).

V. Study III: Harvested Power with a Targeted Value of 1 W

A. Motivation and Objective

In Study I, the number of red LDs required to harvest 1 W using a mono-c-Si cell was estimated to be 61. Also, the experimental levels of the transmitted power were in the order of mW. As a next step, here an array of 42 LDs is designed for the transmission of an amount of optical power able to be converted to 1 W by the mono-c-Si cell. The number of 42 LDs operating at 785 nm is selected because of their ability to transmit larger amounts of power with higher efficiency than the red LDs used in Study I. In order to achieve a maximum harvested power of 1 W, a minimum efficiency of 13.89% is required from the solar cell.

B. Approach

The transmitter of 7.2 W of total optical power is designed in Zemax comprising 42 LDs and collimation lenses. Also, the elliptical Gaussian propagation model presented in Section III is used to support the simulation results given in Section V-E.

C. Simulation Model

The optical design consists of the following objects: source diode, even asphere lens, array and detector rectangle created in the non-sequential components (NSC) mode. Laser diodes and respective aspheric lenses are placed in a rectangular array with perfectly aligned optical axes, as shown in Fig. 15.

The object source diode is used for the simulation of a Panasonic LNCT22PK01WW CW LD. This LD has a typical efficiency of 27.4% and FWHM beam divergences of $\vartheta_{\parallel} = 7.5°$ and $\vartheta_{\perp} = 15°$. According to the model of the source diode, the intensity of the beam generated from a rectangular source is given by:

TABLE IX
Simulation Parameters of 785 nm Laser Diode

Source diode	Parameter	N_{lr}	N_{anr}	$P_{\mathrm{Tx,o}}$	a_{x}	a_{y}
	Unit	-	-	[mW]	[deg]	[deg]
	Value	10^3	10^7	171.1	6.37	12.74
	Parameter	$S_{\mathrm{x}}, S_{\mathrm{y}}$	N_{x}	N_{y}	Δx	Δy
	Unit	-	-	-	[mm]	[mm]
	Value	1	7	6	15.2	16.77

$$G_{\mathrm{s}}(\theta_{\mathrm{x}}, \theta_{\mathrm{y}}) = G_{\mathrm{s},0} \times \times \exp\left\{-2\left[\left(\frac{\theta_{\mathrm{x}}}{a_{\mathrm{x}}}\right)^{2S_{\mathrm{x}}} + \left(\frac{\theta_{\mathrm{y}}}{a_{\mathrm{y}}}\right)^{2S_{\mathrm{y}}}\right]\right\}, \quad (54)$$

where $G_{\mathrm{s},0}$ denotes the overall peak intensity, note that the manufacturers of LDs give the relative instead of the absolute value of intensity; θ_{x} and θ_{y} are the angles in degrees along the x- and y-directions, respectively; and a_{x} and a_{y} are the angular divergences in degrees on the x-z and y-z planes, respectively. The FWHM angular divergences are given by $a_{\mathrm{x}} = \vartheta_{\parallel}/\sqrt{2\ln(2)}$ and $a_{\mathrm{y}} = \vartheta_{\perp}/\sqrt{2\ln(2)}$.

Also, the values of S_{x} and S_{y} are the super-Gaussian factors along the x- and y-axes, respectively and range from 0.01 to 50. The special case of $S_{\mathrm{x}} = S_{\mathrm{y}} = 1$ corresponds to a typical elliptical Gaussian beam. The simulation parameters of the object source diode are given in Table IX. Parameters N_{lr} and N_{anr} denote the number of layout rays and analysis rays, respectively. The term $P_{\mathrm{Tx,o}}$ is used for the output optical power of each LD. Also, N_{x} and N_{y} represent the number of LDs placed along the x- and y-axis, respectively. Finally, Δx and Δy are the distances between the centers of two LDs and lenses placed consecutively along the x- and y-direction, respectively.

The even asphere lens is used for the simulation of a Thorlabs ACL12708U-B lens with an ARC for the wavelength range of 650 nm−1050 nm [67]. The aspheric coefficients of lens are given in [67]. The array object is used for the creation of a rectangular array consisting of 7×6 identical aspheric lenses. An orthogonal descent optimizer is used for the determination of d_0 which denotes the distance between each LD and the input surface of its respective collimation lens. The performance criteria are the maximization of total flux and spatial uniformity. Finally, the value of d_0 is refined by the use of a Hammer optimizer yielding $d_0 = 3.737\,\mathrm{mm}$. A $12.5 \times 12.5\,\mathrm{cm}^2$ rectangular detector modeling the mono-c-Si solar cell is used to measure the received optical power for a distance range of $[1, 100]\,\mathrm{m}$ using increments of 1 m. The material of the detector rectangle is selected to be absorb and the number of pixels along the x- and y-dimension is 150×150.

D. Eye Safety Regulations

1) Single Laser Diode: The LD considered in the simulation model is also classified as Class 3B according to the manufacturer [44]. The MPE in terms of irradiance is calculated to be $\nu = 1.5\,\mathrm{mW/cm}^2$ similar to the methodology presented in Appendix C. Also, the NOHD is determined to

TABLE X
ANALYTICAL PARAMETERS

Parameter	Unit	Value	Parameter	Unit	Value
$P_{\mathrm{Tx,o}}$	[mW]	171.10	$R_{1\mathrm{x}}$	[mm]	3.74
λ_0	[nm]	785.00	$R_{1\mathrm{y}}$	[mm]	3.74
ϑ_{x}	[deg]	3.75	A	-	0.836
ϑ_{y}	[deg]	7.50	B	[mm]	4.93
N_{x}	-	7	C	[cm^{-1}]	1.247
N_{y}	-	6	D	-	0.46
$\Delta\mathrm{x}$	[mm]	15.20	$W_{2\mathrm{x}}$	[μm]	528.19
$\Delta\mathrm{y}$	[mm]	16.77	$W_{2\mathrm{y}}$	[mm]	1.06
$W_{0\mathrm{x}}$	[μm]	3.81	$R_{2\mathrm{x}}$	[m]	-1.38
$W_{0\mathrm{y}}$	[μm]	1.90	$R_{2\mathrm{y}}$	[m]	-1.39
G_0	[MW/cm^2]	1.51	$d_{1\mathrm{x}}$	[cm]	54.63
d_0	[mm]	3.737	$d_{1\mathrm{y}}$	[m]	1.27
$W_{1\mathrm{x}}$	[μm]	244.97	$W_{3\mathrm{x}}$	[μm]	410.15
$W_{1\mathrm{y}}$	[μm]	491.99	$W_{3\mathrm{y}}$	[μm]	311.92

be $d_{\mathrm{NOHD}} = 75\,\mathrm{cm}$ and, therefore, the near infra-red (NIR) beam radiation requires enclosure with a length of 75 cm.

2) Laser Diode and Collimation Lens: The optical transmitter consisting of the LD and lens considered in the simulation model is classified as Class 3B, similar to the methodology presented in Appendix D. The MPE is calculated to be $\nu = 6.66\,\mathrm{mW/cm^2}$ and the NOHD is $d_{\mathrm{NOHD}} = 54.3\,\mathrm{m}$. Therefore, a shielding tube with a length of $54.3\,\mathrm{m}$ is required which is not suitable for practical applications. In order to restrict the NOHD, either the beam diameter should increase by the use of a lens with a larger diameter or the output power of the LD should decrease based on the MPE value.

E. Results and Discussion

The parameters of the analytical model presented in Sections III-B1, III-B2 and III-B3 are used to verify the simulation model and are summarized in Table X. The analytical curves of $\pm W'_{\mathrm{x}}(z)$ and $\pm W'_{\mathrm{y}}(z)$ of a single optical link are shown in Fig. 16(a) and 16(b) for distances up to 5 m and up to 100 m, respectively. These curves are derived by the use of (1)–(10) and (14)–(31). Note that the reference point $z = 0$ denotes the tangent plane to the output surface of the lens and the beam widths refer to the FWHM intensity points. In Fig. 16(a), it is observed that the laser beam along the y- axis focuses on a smaller beam waist at a longer distance and then diverges more than the laser beam along x- axis. The theoretical values of beam divergence expressed at FWHM intensity are calculated to be $\psi_{\mathrm{x}} = 1.22\,\mathrm{mrad}$ and $\psi_{\mathrm{y}} = 1.6\,\mathrm{mrad}$ according to Fig. 16(b). Also, the beam diameters along the x- and y- directions are 12.1 cm and 15.8 cm, respectively, at the link distance of 100 m.

Finally, the received optical power of the 42 laser link is shown as a function of distance in Fig. 17 based on the analytical and simulation model. The two curves are in close agreement, and a maximum gap of 1 dB is observed at the distance of 100 m. According to the analytical model, a value of optical power of 7.15 W is delivered effectively to 20 m. Also, a simulation-based value of 7.13 W is able to be transferred to 10 m. After the distance of 20 m, the analytical curve falls with a larger rate compared with the simulation curve (see Fig. 17). This effect is attributed to the term of $W'_{\mathrm{x}}(z')W'_{\mathrm{y}}(z'')$ that exists in the denominator of (32) in the theoretical model. This term attenuates the irradiance and therefore the optical power faster than the respective irradiance of (54) of the simulation model. Also, the rear surface of the aspheric lens is modeled as spherical in Section III-B2 and this geometrical assumption makes light collimation less efficient. The geometrical losses of optical power are 0.09 dB and 0.1 dB at the link distance of 30 m for the analytical and simulation model, respectively. This means that the particular multiple laser-based link presents a very large collection efficiency of 97.9% and 97.7% at 30 m according to theory and simulation, respectively. The optical-to-electrical efficiency of the particular cell is measured to be 13.25% for an input optical power of 134.38 mW in Experiment III. A received optical power of about 7 W is expected to increase the power conversion efficiency. At the same time the increase in the temperature of the cell is expected to reduce the value of η_{sr} slightly. Overall, the targeted value of 1 W is expected to be achieved in practice by this large amount of received optical power for link distance values of up to 30 m.

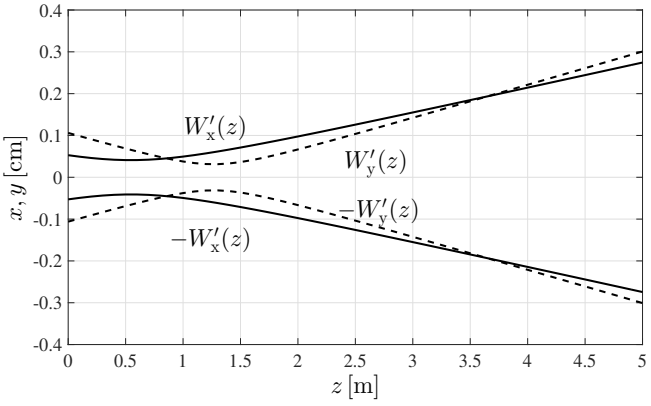

(a)

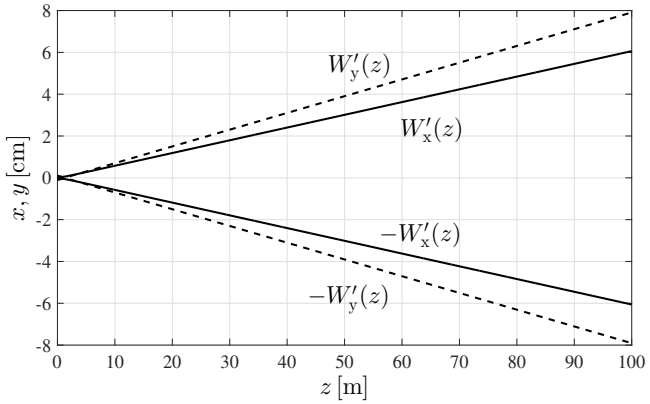

(b)

Fig. 16. Theoretical full width at half maximum (FWHM) intensity of the single laser beam versus distance up to (a) 5 m and (b) 100 m along x- and y- axes.

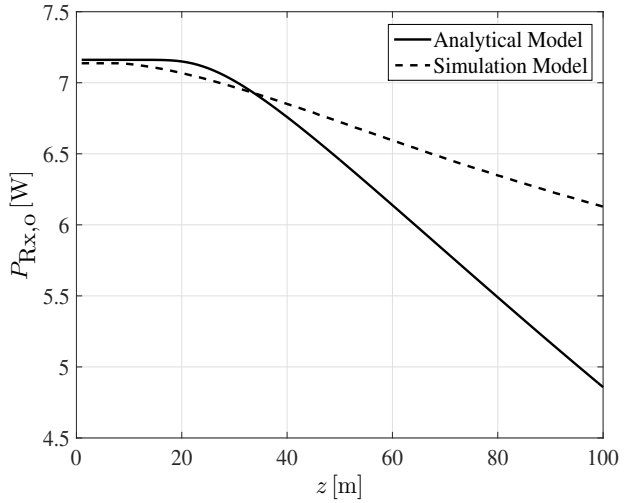

Fig. 17. Received optical power versus distance for two different models.

VI. Summary and Conclusions

In this comprehensive study, the application of the principle of OWPT to SCs was investigated for the first time for an indoor scenario during darkness hours, i.e. in the absence of ambient light.

In particular, an experimental study was undertaken to determine the maximum link efficiency, maximum harvested power and optical receiver efficiency. The optical sources were up to four red CW LDs combined with the use of aspheric lenses for beam collimation. The optical receivers were a solar panel and a solar cell based on the technology of multi-c-Si and mono-c-Si, respectively. The link distance was 5.2 m. A high energy efficiency with a fill factor of 69% and a harvested electrical power of 30.6 mW was attained by the solar panel. The best value of maximum link efficiency of 3.2% was achieved by two optical transmitters and the solar cell. This relatively low value was explained by the contribution of the low measured average efficiency of the 2 LDs of 26.8% and the solar cell efficiency of 13.3%. For the same link, the geometrical losses of optical power were estimated to be only 10.6% and this fact was sufficient to characterize the optical link as highly efficient with OWPT showing great potential at longer distances. However, the analytical calculation of the MPE and NOHD for eye safety resulted in the need for a beam enclosure of up to 3.6 m. Also, a comparison was made for the same OW link with a state-of-the-art IPTS with optimally shaped dipole coils. As a result, a performance improvement in terms of total power efficiency by 2.7 times was achieved by the link consisting of 2 LDs and a solar cell. Therefore, the applicability of indoor OWPT to SCs was demonstrated with an acceptable link efficiency and the possibility of extending the distance of 5.2 m.

Another experimental study was undertaken for the determination of the laser beam divergence with a targeted value of 1 mrad. In particular, an optical transmitter was created by the use of the red LD and a spherical lens. Also, an analytical model was developed for the prediction of the elliptical Gaussian beam propagation and was applied to the experimental data for curve fitting and estimation of its unknown parameters. As a result, the divergence of full width at 36.8% of peak intensity was determined to be 3 mrad and 5.75 mrad along the 'slow' and 'fast' axes of the laser beam, respectively. Moreover, the beam divergence determined by the diameter of the circular image was measured to be only 2.1 mrad. Thus, this single optical link was characterized by high directivity enabling the application of OWPT to longer distances.

The best maximum harvested power measured in the experiments was 30.6 mW. This provided the basis for the determination of the number of LDs needed to achieve the target of 1 W which is required for the operation of small RF cells. This led to a 42 laser-based transmitter of 7.2 W that transfers power to the mono-c-Si cell placed up to 100 m. The system was designed by the use of the simulation tool Zemax and the respective theoretical model of Gaussian beam propagation. The beam divergence defined by the FWHM intensity was analytically determined to be 1.2 mrad and 1.6 mrad along the 'slow' and 'fast' axes, respectively. In addition to this large directivity, the simulation and analytical models were in close agreement showing that the transfer of 7.2 W up to 30 m with geometrical losses of only 2% was feasible. Therefore, the minimum required efficiency of the solar cell was only 13.9%, while an efficiency of 13.3% was measured in the experiments for an input optical power of 134.4 mW. However, a beam enclosure was required due to eye safety restrictions.

Finally, in a practical outdoor scenario of power supply to a SC, the great potential of harvesting sunlight power in addition to WPT from 'dedicated' laser sources remains unresearched. This important advantage of solar cells over rectennas, harvesting additional power from a natural source as well as from human-made EM sources, gives the opportunity for a wide application of the principle of OWPT.

Appendix A
Motivation for a Gaussian Beam Model and Paraxial Approximation

The manufacturers' data sheets for LDs give a graph of the far field relative intensity versus the parallel and perpendicular to the junction angular divergence of the beam. These angular divergence graphs can be approximated by Gaussian curves of different widths for the LDs considered in this research [43], [44]. Also, the selected LDs operate at the fundamental transverse electrical (TE) mode. Therefore, an elliptical Gaussian beam propagation model is considered for the generated laser beam [41].

Ray optics, also known as geometrical optics, is the simplest theory that describes light propagation [46]. According to this theory, light consists of optical rays traveling from one medium to another under defined geometrical rules. Optical rays are described by their position in space and inclination. In paraxial optics, a subset of ray optics, rays propagate at small angles from an optical axis, which the optical components are aligned with. Also, in wave optics, waves with wavefront normals forming small angles with the propagation z- axis are called paraxial. These waves satisfy the paraxial Helmholtz equation [68]. A well known and

useful solution of this equation is the Gaussian beam. Paraxial optics is used in first-order ray tracing and Gaussian optics. In particular, the paraxial approximation is used and is described by the properties: $\sin(\vartheta) \approx \vartheta$, $\tan(\vartheta) \approx \vartheta$ and $\cos(\vartheta) \approx 1$, where ϑ [rad] is the angle between the optical axis and the ray.

APPENDIX B
MATHEMATICAL DERIVATION OF (12) AND (43)

The total optical power of the beam is expressed as the double integral over the transverse x-y plane by:

$$\begin{aligned} P_{\text{Tx,o}} &= \int_{-\infty}^{\infty}\int_{-\infty}^{\infty} G(x,y,z)\mathrm{d}x\mathrm{d}y \\ &= G_0 \frac{W_{0\text{x}}W_{0\text{y}}}{W_{\text{x}}(z)W_{\text{y}}(z)} \int_{-\infty}^{\infty} \exp\left[\frac{-2x^2}{W_{\text{x}}^2(z)}\right]\mathrm{d}x\times \\ &\quad \times \int_{-\infty}^{\infty} \exp\left[\frac{-2y^2}{W_{\text{y}}^2(z)}\right]\mathrm{d}y \\ &= G_0 \frac{W_{0\text{x}}W_{0\text{y}}}{W_{\text{x}}(z)W_{\text{y}}(z)} \int_{0}^{\infty} 2\exp\left[\frac{-2x^2}{W_{\text{x}}^2(z)}\right]\mathrm{d}x\times \\ &\quad \times \int_{0}^{\infty} 2\exp\left[\frac{-2y^2}{W_{\text{y}}^2(z)}\right]\mathrm{d}y. \end{aligned} \tag{55}$$

The two exponential integrals of the second part of (55) yield the following result [69]:

$$\begin{aligned} P_{\text{Tx,o}} &= G_0 \frac{W_{0\text{x}}W_{0\text{y}}}{W_{\text{x}}(z)W_{\text{y}}(z)} W_{\text{x}}(z)\sqrt{\frac{\pi}{2}}W_{\text{y}}(z)\sqrt{\frac{\pi}{2}} \\ &= \frac{\pi}{2} G_0 W_{0\text{x}}W_{0\text{y}}. \end{aligned} \tag{56}$$

The ratio of the optical power collected by a rectangular optical receiver with the dimensions of $2x_0 \times 2y_0$ at a distance $z \geq d_0 + t_{\text{c}}$ over the total optical power can be expressed by:

$$\begin{aligned} \eta_{\text{c}}(z) &= \frac{1}{(1-r)P_{\text{Tx,o}}} \int_{-x_0}^{x_0}\int_{-y_0}^{y_0} G'(x,y,z)\mathrm{d}x\mathrm{d}y \\ &\overset{(32)}{=} \frac{2}{\pi W'_{\text{x}}(z')W'_{\text{y}}(z'')} \int_{-x_0}^{x_0} \exp\left[\frac{-2x^2}{W'^2_{\text{x}}(z')}\right]\mathrm{d}x\times \\ &\quad \times \int_{-y_0}^{y_0} \exp\left[\frac{-2y^2}{W'^2_{\text{y}}(z'')}\right]\mathrm{d}y \\ &= \frac{2}{\pi W'_{\text{x}}(z')W'_{\text{y}}(z'')} \int_{0}^{x_0} 2\exp\left[\frac{-2x^2}{W'^2_{\text{x}}(z')}\right]\mathrm{d}x\times \\ &\quad \times \int_{0}^{y_0} 2\exp\left[\frac{-2y^2}{W'^2_{\text{y}}(z'')}\right]\mathrm{d}y. \end{aligned} \tag{57}$$

Again, the two exponential integrals of the second part of (57) result in [69]:

$$\begin{aligned} \eta_{\text{c}}(z) &= \frac{2}{\pi W'_{\text{x}}(z')W'_{\text{y}}(z'')} W'_{\text{x}}(z')\frac{\pi}{2}\mathrm{erf}\left[\frac{\sqrt{2}x_0}{W'_{\text{x}}(z')}\right]\times \\ &\quad \times W'_{\text{y}}(z'')\mathrm{erf}\left[\frac{\sqrt{2}y_0}{W'_{\text{y}}(z'')}\right] \\ &= \mathrm{erf}\left[\frac{\sqrt{2}x_0}{W'_{\text{x}}(z')}\right]\mathrm{erf}\left[\frac{\sqrt{2}y_0}{W'_{\text{y}}(z'')}\right]. \end{aligned} \tag{58}$$

APPENDIX C
CLASSIFICATION OF THE SINGLE LASER DIODE

The maximum output optical power of the LD is $P_{\text{Tx,o,m}} = 130\,\text{mW}$ [43]. The beam diameter is defined in BS EN 60825-1:2014 [11] as the smallest circle that contains 63% of the total laser power, i.e. $1/e$ beam width. Also, the beam divergence is defined as the far field plane angle of the cone created by the beam diameter. So long as the LD has a Gaussian elliptical profile, the beam divergences are defined along the x- and y- axes as $\varphi_{\text{x}} = 2\vartheta_{\text{x}}$ and $\varphi_{\text{y}} = 2\vartheta_{\text{y}}$, respectively. In particular, they are calculated to be $\varphi_{\text{x}} = 12.5° \simeq 0.22\,\text{rad}$ and $\varphi_{\text{y}} = 21.2° \simeq 0.37\,\text{rad}$ from [43]. According to (1) and (2) the beam diameters along the x- and y- axes can be calculated up to the $1/e \simeq 0.37$ points of the intensity pattern. In particular, the application of $\lambda_0 = 0.66\,\mu\text{m}$, $\vartheta_{\text{x}} = 6.25°$ and $\vartheta_{\text{y}} = 10.6°$ to (1) and (2) results in $W_{0\text{x}} = 1.92\,\mu\text{m}$ and $W_{0\text{y}} = 1.12\,\mu\text{m}$, respectively. Therefore, the beam diameters along the x- and y- directions are calculated to be $D_{0\text{x}} = 2W_{0\text{x}} = 3.84\,\mu\text{m}$ and $D_{0\text{y}} = 2W_{0\text{y}} = 2.24\,\mu\text{m}$, respectively.

Condition 3 of Table 10 [11] can be applied to the selected optical emitter. The measurement of AEL needs to be made by the use of a circular aperture stop with a diameter of $D_{\text{ap}} = 7\,\text{mm}$ at a distance $d_{\text{m}} = 10\,\text{cm}$ from the optical source. The specific LD is divergent and the elliptical beam has larger dimensions than the circular area of the aperture stop. Therefore, the AEL must be expressed in terms of irradiance (in mW/cm^2) rather than optical power (in mW). The angular subtenses along the x- and y- axes can be found from:

$$\alpha_{\text{x}} = 2\tan^{-1}\left(\frac{D_{0\text{x}}}{2d_{\text{m}}}\right) \approx \frac{D_{0\text{x}}}{d_{\text{m}}} \tag{59}$$

and

$$\alpha_{\text{y}} = 2\tan^{-1}\left(\frac{D_{0\text{y}}}{2d_{\text{m}}}\right) \approx \frac{D_{0\text{y}}}{d_{\text{m}}}. \tag{60}$$

In particular, applying the values of $D_{0\text{x}} = 3.84\,\mu\text{m}$, $D_{0\text{y}} = 2.24\,\mu\text{m}$ and $d_{\text{m}} = 10^5\,\mu\text{m}$ to (59) and (60), the angular subtenses are calculated to be $\alpha_{\text{x}} = 38.4\,\mu\text{rad} < \alpha_{\text{min}} = 1.5\,\text{mrad}$ and $\alpha_{\text{y}} = 22.4\,\mu\text{rad} < \alpha_{\text{min}}$, respectively. Note that the classification principle 4.3 d) of [11] states that the angular subtense of a rectangular source is computed by the arithmetic mean value of the two angular dimensions of the source. Also, any value of the angular subtense smaller than α_{min} or bigger than $\alpha_{\text{max}} = 100\,\text{mrad}$ needs to be limited to α_{min} or α_{max}, respectively, before the calculation of mean value. Therefore, $\alpha = (1.5 + 1.5)/2 = 1.5\,\text{mrad}$ and the LD is assumed to be a point source.

Assume that the LD can be classified as Class 3R and select a time base of $0.25\,\text{s}$ according to the classification principle 4.3 e) of [11]. Then, the correction factor, C_6, is equal to 1 according to Table 9 [11]. Therefore, the AEL is determined to be $\kappa = 5\,\text{mW}$ based on Table 6 [11]. The AEL expressed as irradiance is computed by:

$$G_{\text{AEL}} = \frac{\kappa}{\pi(D_{\text{ap}}/2)^2}. \tag{61}$$

The application of $\kappa = 5\,\text{mW}$ and $D_{\text{ap}} = 0.7\,\text{cm}$ to (61) results in $G_{\text{AEL}} \simeq 13\,\text{mW/cm}^2$.

Now, the beam irradiance must be determined at $d_{\text{m}} = 10\,\text{cm}$ from the LD chip and be compared with G_{AEL}. For

this reason, the beam diameter along the x- and y- axes is calculated by the use of (3) and (4), respectively. The application of $z = d_{\rm m} = 10\,{\rm cm}$, $W_{0{\rm x}} = 1.92\,\mu{\rm m}$ and $\lambda_0 = 0.66\,\mu{\rm m}$ to (3) yields $W_{\rm x}(10\,{\rm cm}) = 10.94\,{\rm mm}$. Also, the values of $z = d_{\rm m} = 10\,{\rm cm}$, $W_{0{\rm y}} = 1.12\,\mu{\rm m}$ and $\lambda_0 = 0.66\,\mu{\rm m}$ are applied to (4) and they result in $W_{\rm y}(10\,{\rm cm}) = 18.76\,{\rm mm}$. Therefore, the beam diameters at $d_{\rm m} = 10\,{\rm cm}$ are $D_{\rm x}(10\,{\rm cm}) = 2W_{\rm x}(10\,{\rm cm}) = 21.88\,{\rm mm}$ and $D_{\rm y}(10\,{\rm cm}) = 2W_{\rm y}(10\,{\rm cm}) = 37.52\,{\rm mm}$. The geometry of the circular aperture is approximated by that of a square aperture with side length equal to the diameter of the circular aperture, i.e. $2x_0 = 2y_0 = 7\,{\rm mm}$. In this case, the collection efficiency can be expressed based on (43) by:

$$\eta_{\rm c}(z) = {\rm erf}\left[\frac{\sqrt{2}x_0}{W_{\rm x}(z)}\right]{\rm erf}\left[\frac{\sqrt{2}y_0}{W_{\rm y}(z)}\right], \tag{62}$$

where $W_{\rm x}(z)$ and $W_{\rm y}(z)$ are given by (3) and (4), respectively. The values of $z = d_{\rm m} = 10\,{\rm cm}$, $x_0 = y_0 = 3.5\,{\rm mm}$, $W_{\rm x}(10\,{\rm cm}) = 10.94\,{\rm mm}$ and $W_{\rm y}(10\,{\rm cm}) = 18.76\,{\rm mm}$ are applied to (62) resulting in $\eta_{\rm c}(10\,{\rm cm}) = 0.139$. Therefore, the received optical power is $P_{\rm Rx,o}(10\,{\rm cm}) = \eta_{\rm c}(10\,{\rm cm})P_{\rm Tx,o,m} = 0.139\times 130 = 18.07\,{\rm mW}$. Finally, the received beam irradiance from a square aperture of side length $2x_0$ is given by:

$$G_{\rm Rx}(z) = \frac{P_{\rm Rx,o}(z)}{(2x_0)^2}. \tag{63}$$

The application of $z = d_0 = 10\,{\rm cm}$, $P_{\rm Rx,o}(10\,{\rm cm}) = 18.07\,{\rm mW}$ and $2x_0 = 0.7\,{\rm cm}$ to (63) results in $G_{\rm Rx}(10\,{\rm cm}) = 36.88\,{\rm mW/cm^2}$. This value is larger than $G_{\rm AEL}$. Consequently, the LD cannot be classified as Class 3R.

Now, the LD is considered to belong to Class 3B, and a time base of $100\,{\rm s}$ is selected according to the classification principle 4.3 e). The received optical power, i.e. $P_{\rm Rx,o}(10\,{\rm cm}) = 18.07\,{\rm mW}$, is less than the AEL, i.e. $\kappa = 0.5\,{\rm W}$, derived from Table 8. As a result, the optical source is classified as Class 3B.

APPENDIX D
CLASSIFICATION OF THE LASER DIODE USED WITH COLLIMATION LENS

In this case, the laser consists of the DC power supply, the LD and the aspheric lens used in Scenario II of Experiment II. So long as the area between the LD and the lens is shielded by an aluminum tube, the total optical device is considered to be an extended optical source. Note that Condition 1 of Table 10 [11] is applicable to collimated beams, but the most restrictive condition must be used for classification and, again, this is Condition 3 of Table 10 [11]. Thus, the measurement of AEL needs to be made by the use of a circular aperture stop with a diameter of $D_{\rm ap} = 7\,{\rm mm}$ at a distance of $d_{\rm m} = 10\,{\rm cm}$ from the new beam waist according to Table 11 [11]. As a first step, the new beam waists must be determined. The application of the values of parameters presented in Table II to (1)–(10) and (14)–(29) results in $W_{3{\rm x}} = 34.93\,\mu{\rm m}$ and $W_{3{\rm y}} = 20.39\,\mu{\rm m}$. Therefore, the substitution of $z' = d_{\rm m} = 10\,{\rm cm}$, $W_{3{\rm x}} = 34.93\,\mu{\rm m}$ and $\lambda_0 = 660\,{\rm nm}$ to (30) gives $W'_{\rm x}(10\,{\rm cm}) = 602.46\,\mu{\rm m}$. Also, the values of $z'' = d_{\rm m} = 10\,{\rm cm}$, $W_{3{\rm y}} = 20.39\,\mu{\rm m}$ and $\lambda_0 = 660\,{\rm nm}$ are applied to (31) and yield $W'_{\rm y}(10\,{\rm cm}) = 1.03\,{\rm mm}$. So long as the beam diameters at $10\,{\rm cm}$ from the beam waists are smaller than the diameter of the circular stop aperture, the AEL can be expressed as power and not as irradiance. The angular subtenses along the x- and y- axes are given by:

$$\alpha_{\rm x} = 2\tan^{-1}\left[\frac{W'_{\rm x}(d_{\rm m})}{d_{\rm m}}\right] \approx \frac{2W'_{\rm x}(d_{\rm m})}{d_{\rm m}} \tag{64}$$

and

$$\alpha_{\rm y} = 2\tan^{-1}\left[\frac{W'_{\rm y}(d_{\rm m})}{d_{\rm m}}\right] \approx \frac{2W'_{\rm y}(d_{\rm m})}{d_{\rm m}}. \tag{65}$$

The application of $W'_{\rm x}(10\,{\rm cm}) = 602.46\,\mu{\rm m}$, $W'_{\rm y}(10\,{\rm cm}) = 1.03\,{\rm mm}$ and $d_{\rm m} = 10\,{\rm cm}$ to (64) and (65) results in $\alpha_{\rm x} = 12\,{\rm mrad}$ and $\alpha_{\rm y} = 20.6\,{\rm mrad}$, respectively. Therefore, $\alpha = (\alpha_{\rm x} + \alpha_{\rm y})/2 = 16.3\,{\rm mrad}$.

Assume that the optical transmitter can be classified as Class 3R, and select a time base of $0.25\,{\rm s}$ according to the classification principle 4.3 e) of [11]. Then, the correction factor C_6 is equal to $\alpha/\alpha_{\rm min} = 10.867$ according to Table 9 [11]. Therefore, the AEL is determined to be $\kappa = 5C_6\,[{\rm mW}]$ based on Table 7 [11] and, finally, $\kappa = 54.34\,{\rm mW}$.

Now, the laser beam power needs to be calculated at $10\,{\rm cm}$ from the beam waists in order to be compared with the AEL of Class 3R. So long as $d_{1{\rm x}} \simeq d_{1{\rm y}}$ according to Table II, the collection efficiency of the rectangular receiver is calculated at $z' \simeq z'' = 10\,{\rm cm}$. The application of $x_0 = y_0 = 3.5\,{\rm mm}$, $W'_{\rm x}(10\,{\rm cm}) = 602.46\,\mu{\rm m}$ and $W'_{\rm y}(10\,{\rm cm}) = 1.03\,{\rm mm}$ to (43) gives a collection efficiency value of $\eta_{\rm c}(10\,{\rm cm}) = 1$, as expected. So, the received optical power is $P_{\rm Rx,o}(10\,{\rm cm}) = P_{\rm Tx,o,m} = 130\,{\rm mW}$ that is larger than $\kappa = 54.34\,{\rm mW}$. Therefore, again this optical transmitter is not classified as Class 3R, but as Class 3B. This is because the AEL of Class 3B is $\kappa = 500\,{\rm mW}$.

ACKNOWLEDGMENT

The authors acknowledge partial financial support by Bell Labs, Nokia Ireland. Professor Haas acknowledges support from the Engineering and Physical Sciences Research Council (EPSRC) under the Established Career Fellowship grant EP/K008757/1.

REFERENCES

[1] H. Claussen, L. T. Ho, and L. G. Samuel, "An Overview of the Femtocell Concept," *Bell Labs Tech. J.*, vol. 13, no. 1, pp. 221–245, Spring 2008.
[2] W. Webb, *Wireless Communications: The Future*. New York, NY, USA: Wiley, Jan. 2007.
[3] R. Razavi and H. Claussen, "Urban Small Cell Deployments: Impact on the Network Energy Consumption," in *Proc. IEEE Wireless Commun. Netw. Conf. Workshops*, Paris, France, Apr. 2012, pp. 47–52.
[4] C. Ranaweera *et al.*, "Design and Optimization of Fiber Optic Small-Cell Backhaul Based on an Existing Fiber-to-the-Node Residential Access Network," *IEEE Commun. Mag.*, vol. 51, no. 9, pp. 62–69, Sep. 2013.
[5] Y. Mao, Y. Luo, J. Zhang, and K. Letaief, "Energy Harvesting Small Cell Networks: Feasibility, Deployment, and Operation," *IEEE Commun. Mag.*, vol. 53, no. 6, pp. 94–101, June 2015.
[6] N. Tesla, "The Transmission of Electrical Energy without Wires as a Means for Furthering Peace," *Elect. World Eng.*, pp. 21–24, Jan. 1905.
[7] H. Elgala, R. Mesleh, and H. Haas, "Indoor Optical Wireless Communication: Potential and State-of-the-Art," *IEEE Commun. Mag.*, vol. 49, no. 9, pp. 56–62, Sep. 2011.

[8] J. Fakidis, M. Ijaz, S. Kucera, H. Claussen, and H. Haas, "On the Design of an Optical Wireless Link for Small Cell Backhaul Communication and Energy Harvesting," in *Proc. IEEE 25th Annu. Int. Symp. Personal Indoor Mobile Radio Commun.*, Washington, DC, USA, Sept. 2014, pp. 58–62.

[9] J. Fakidis, S. Kucera, H. Claussen, and H. Haas, "On the Design of a Free Space Optical Link for Small Cell Backhaul Communication and Power Supply," in *Proc. IEEE Int. Conf. Commun. Workshop*, London, U.K., June 2015, pp. 1428–1433.

[10] C. Park, S. Lee, G.-H. Cho, and C. Rim, "Innovative 5-m-Off-Distance Inductive Power Transfer Systems with Optimally Shaped Dipole Coils," *IEEE Trans. Power Electron.*, vol. 30, no. 2, pp. 817–827, Feb. 2015.

[11] *Safety of Laser Products. Equipment Classification and Requirements*, British Standards Institution (BSI) Std. BS EN 60 825-1:2014, Aug. 2014.

[12] A. Bauer, J. Hanisch, and E. Ahlswede, "An Effective Single Solar Cell Equivalent Circuit Model for Two or More Solar Cells Connected in Series," *IEEE J. Photovolt.*, vol. 4, no. 1, pp. 340–347, Jan. 2014.

[13] C. R. Valenta and G. D. Durgin, "Harvesting Wireless Power: Survey of Energy-Harvester Conversion Efficiency in Far-Field Wireless Power Transfer Systems," *IEEE Microw. Mag.*, vol. 15, no. 4, pp. 108–120, May 2014.

[14] X. Lu, P. Wang, D. Niyato, D. I. Kim, and Z. Han, "Wireless Networks with RF Energy Harvesting: A Contemporary Survey," *IEEE Commun. Surveys Tuts.*, vol. 17, no. 2, pp. 757–789, Apr.–Jun. 2015.

[15] A. Kurs *et al.*, "Wireless Power Transfer via Strongly Coupled Magnetic Resonances," *Sci.*, vol. 317, no. 5834, pp. 83–86, Jul. 2007.

[16] B. Choi, E. Lee, J. Huh, and C. Rim, "Lumped Impedance Transformers for Compact and Robust Coupled Magnetic Resonance Systems," *IEEE Trans. Power Electron.*, vol. 30, no. 11, pp. 6046–6056, Nov. 2015.

[17] M. Pinuela, D. Yates, S. Lucyszyn, and P. Mitcheson, "Maximizing DC-to-Load Efficiency for Inductive Power Transfer," *IEEE Trans. Power Electron.*, vol. 28, no. 5, pp. 2437–2447, May 2013.

[18] T. Le, K. Mayaram, and T. Fiez, "Efficient Far-Field Radio Frequency Energy Harvesting for Passively Powered Sensor Networks," *IEEE J. Solid-State Circuits*, vol. 43, no. 5, pp. 1287–1302, May 2008.

[19] R. Dickinson, "Power in the Sky: Requirements for Microwave Wireless Power Beamers for Powering High-Altitude Platforms," *IEEE Microw. Mag.*, vol. 14, no. 2, pp. 36–47, Mar. 2013.

[20] L. Summerer and O. Purcell, "Concepts for Wireless Energy Trasmission via Laser," presented at the 1st Int. Conf. Space Opt. Syst. Appl., Tokyo, Japan, Feb. 2009.

[21] A. Sahai and D. Graham, "Optical Wireless Power Transmission at Long Wavelengths," in *Proc. IEEE Int. Conf. Space Opt. Syst. Appl.*, Santa Monica, CA, USA, May 2011, pp. 164–170.

[22] W. C. Brown, "The History of Power Transmission by Radio Waves," *IEEE Trans. Microw. Theory Techn.*, vol. 32, no. 9, pp. 1230–1242, Sep. 1984.

[23] M. Pinuela, P. Mitcheson, and S. Lucyszyn, "Ambient RF Energy Harvesting in Urban and Semi-Urban Environments," *IEEE Trans. Microw. Theory Techn.*, vol. 61, no. 7, pp. 2715–2726, Jul. 2013.

[24] V. Marian, B. Allard, C. Vollaire, and J. Verdier, "Strategy for Microwave Energy Harvesting From Ambient Field or a Feeding Source," *IEEE Trans. Power Electron.*, vol. 27, no. 11, pp. 4481–4491, Nov. 2012.

[25] P. E. Glaser, "Power from the Sun: Its Future," *Sci.*, vol. 162, no. 3856, pp. 857–861, Nov. 1968.

[26] P. Crump *et al.*, "Efficient High-Power Laser Diodes," *IEEE J. Sel. Topics Quantum Electron.*, vol. 19, no. 4, pp. 1 501 211–1 501 211, Jul. 2013.

[27] J. L. Gray, "The Physics of the Solar Cell," in *Handbook of Photovoltaic Science and Engineering*, 2nd ed. New York, NY, USA: Wiley, June 2011, pp. 82–129.

[28] M. A. Green, K. Emery, Y. Hishikawa, W. Warta, and E. D. Dunlop, "Solar Cell Efficiency Tables (Version 46)," *Progress Photovolt., Res. Appl.*, vol. 23, no. 7, pp. 805–812, Jul. 2015.

[29] G. Kinsey, A. Nayak, M. Liu, and V. Garboushian, "Increasing Power and Energy in Amonix CPV Solar Power Plants," *IEEE J. Photovolt.*, vol. 1, no. 2, pp. 213–218, Oct. 2011.

[30] M. Ali, G. Yang, and R. Dougal, "A New Circularly Polarized Rectenna for Wireless Power Transmission and Data Communication," *IEEE Antennas Wireless Propag. Lett.*, vol. 4, pp. 205–208, 2005.

[31] X.-X. Yang, C. Jiang, A. Elsherbeni, F. Yang, and Y.-Q. Wang, "A Novel Compact Printed Rectenna for Data Communication Systems," *IEEE Trans. Antennas Propag.*, vol. 61, no. 5, pp. 2532–2539, May 2013.

[32] S. Dimitrov and H. Haas, "Information Rate of OFDM-Based Optical Wireless Communication Systems With Nonlinear Distortion," *IEEE J. Lightw. Technol.*, vol. 31, no. 6, pp. 918–929, Mar. 2013.

[33] A. Hussein and J. Elmirghani, "Mobile Multi-Gigabit Visible Light Communication System in Realistic Indoor Environment," *IEEE J. Lightw. Technol.*, vol. 33, no. 15, pp. 3293–3307, Aug. 2015.

[34] D. Tsonev, H. Chun, S. Rajbhandari, J. McKendry, S. Videv, E. Gu, M. Haji, S. Watson, A. Kelly, G. Faulkner, M. Dawson, H. Haas, and D. O'Brien, "A 3-Gb/s Single-LED OFDM-Based Wireless VLC Link Using a Gallium Nitride μLED," *IEEE Photon. Technol. Lett.*, vol. 26, no. 7, pp. 637–640, Apr. 2014.

[35] Z. Wang, D. Tsonev, S. Videv, and H. Haas, "On the Design of a Solar-Panel Receiver for Optical Wireless Communications with Simultaneous Energy Harvesting," *IEEE J. Sel. Areas Commun.*, vol. 33, no. 8, pp. 1612–1623, Aug. 2015.

[36] S.-M. Kim and J.-S. Won, "Simultaneous Reception of Visible Light Communication and Optical Energy Using a Solar Cell Receiver," in *Proc. IEEE Int. Conf. ICT Convergence*, Jeju Island, South Korea, Oct. 2013, pp. 896–897.

[37] S. Bloom, E. Korevaar, J. Schuster, and H. Willebrand, "Understanding the Performance of Free-Space Optics [Invited]," *OSA J. Opt. Netw.*, vol. 2, no. 6, pp. 178–200, Jun. 2003.

[38] D. K. Killinger, J. H. Churnside, and L. S. Rothman, "Atmospheric Optics," in *Handbook of Optics: Volume V – Atmospheric Optics, Modulators, Fiber Optics, X-Ray and Neutron Optics*, 3rd ed. New York, NY, USA: McGraw-Hill, 2010, pp. 1–50.

[39] A. Mostafa and S. Hranilovic, "Channel Measurement and Markov Modeling of an Urban Free-Space Optical Link," *IEEE/OSA J. Opt. Commun. Netw.*, vol. 4, no. 10, pp. 836–846, Oct. 2012.

[40] F. S. Vetelino, C. Young, L. Andrews, and J. Recolons, "Aperture Averaging Effects on the Probability Density of Irradiance Fluctuations in Moderate-to-Strong Turbulence," *OSA J. Appl. Opt.*, vol. 46, no. 11, pp. 2099–2108, Apr. 2007.

[41] B. E. A. Saleh and M. C. Teich, "Beam Optics," in *Fundamentals of Photonics*, 1st ed., ser. Wiley in Pure and Applied Optics. New York, NY, USA: Wiley, Jan. 1991, pp. 80–107.

[42] ——, "Semiconductor Photon Sources," in *Fundamentals of Photonics*, 1st ed., ser. Wiley in Pure and Applied Optics. New York, NY, USA: Wiley, Jan. 1991, pp. 592–643.

[43] Opnext, "HL6544FM Visible High Power Laser Diodes," Mar. 2009. [Online]. Available: http://www.thorlabs.de/thorcat/21700/HL6544FM-MFGSpec.pdf. Accessed on: May 19, 2014.

[44] Panasonic, "Laser Diode LNCT22PK01WW," Sep. 2013. [Online]. Available: http://docs-europe.electrocomponents.com/webdocs/1305/0900766b81305a62.pdf. Accessed on: Feb. 27, 2015.

[45] J. Alda, "Laser and Gaussian Beam Propagation and Transformation," *Encyclopedia Opt. Eng.*, pp. 999–1013, 2003.

[46] B. E. A. Saleh and M. C. Teich, "Ray Optics," in *Fundamentals of Photonics*, 1st ed., ser. Wiley in Pure and Applied Optics. New York, NY, USA: Wiley, Jan. 1991, pp. 1–40.

[47] D. M. Pozar, *Microwave Engineering*, 4th ed., A. Melhorn, Ed. New York, NY, USA: Wiley, Dec. 2011.

[48] E. Hecht, *Optics*, 4th ed., A. Black, Ed. Reading, MA, USA: Addison-Wesley, 2002.

[49] S. Boyd and L. Vandenberghe, *Convex Optimization*. Cambridge, U.K.: Cambridge Univ. Press, 2004.

[50] A. Sellami and M. Bouaicha, "Application of the Genetic Algorithms for Identifying the Electrical Parameters of PV Solar Generators," in *Solar Cells – Silicon Wafer-Based Technologies*. West Palm Beach, FL, USA: InTech, 2011, pp. 349–364.

[51] D. Killinger, "Free Space Optics for Laser Communication through the Air," *Opt. Photon. News*, vol. 13, no. 3, pp. 36–42, Oct. 2002.

[52] M. Villalva, J. Gazoli, and E. Filho, "Comprehensive Approach to Modeling and Simulation of Photovoltaic Arrays," *IEEE Trans. Power Electron.* , vol. 24, no. 5, pp. 1198–1208, May 2009.

[53] I. Tobias, C. del Canizo, and J. Alonso, "Crystalline Silicon Solar Cells and Modules," in *Handbook of Photovoltaic Science and Engineering*, 2nd ed. New York, NY, USA: Wiley, Jun. 2011, pp. 265–308.

[54] Thorlabs, "ACL12708U-A – Aspheric Condenser Lens, AR-Coated $350 - 700\,\text{nm}$, $D = 1.27\,\text{cm}$, $f = 8\,\text{mm}$," Nov. 2013. [Online]. Available: http://www.thorlabs.de/thorcat/CTN/ACL12708U-A-AutoCADPDF.pdf. Accessed on: May 22, 2014.

[55] Multicomp, "MC-SP0.8-NF-GCS Solar Panel, 0.8 W, 4 V, No Frame," Dec. 2010. [Online]. Available: http://www.farnell.com/datasheets/1671797.pdf. Accessed on: Jun. 11, 2015.

[56] Ebay, "$125\times125\,\text{mm}^2$ Monocrystalline Solar Cells 2.91 W Mono 5×5," Dec. 2014. [Online]. Available: http://www.ebay.co.uk/itm/125x125-Monocrystalline-Solar-Cells-

2-91-Watt-Mono-5x5-/221545517144?item=221545517144&ssPageName=ADME:L:OC:GB:%20\\3160. Accessed on: Jun. 11, 2015.

[57] S. Chander, A. Purohit, A. Nehra, S. P. Nehra, and M. S. Dhaka, "A Study on Spectral Response and External Quantum Efficiency of Mono-Crystalline Silicon Solar Cell," *Int. J. Renewable Energy Res.*, vol. 5, no. 1, pp. 41–44, 2015.

[58] Y. Baghzouz, "Basic Photovoltaic Theory," in *Handbook of Clean Energy Systems*, 1st ed. New York, NY, USA: Wiley, Jun. 2015, pp. 283–296.

[59] H. Schmidt, B. Burger, and J. Schmid, "Power Conditioning for Photovoltaic Power Systems," in *Handbook of Photovoltaic Science and Engineering*, 2nd ed. New York, NY, USA: Wiley, Jun. 2011, pp. 954–983.

[60] J. D. Arora, A. V. Verma, and M. Bhatnagar, "Variation of Series Resistance with Temperature and Illumination Level in Diffused Junction Poly- and Single-Crystalline Silicon Solar Cells," *J. Mater. Sci. Lett.*, vol. 5, no. 12, pp. 1210–1212, Dec. 1986.

[61] F. Khan, S. N. Singh, and M. Husain, "Effect of Illumination Intensity on Cell Parameters of a Silicon Solar Cell," *J. Solar Energy Mater. Solar Cells*, vol. 94, no. 9, pp. 1473–1476, Sep. 2010.

[62] B. E. A. Saleh and M. C. Teich, "Photons and Atoms," in *Fundamentals of Photonics*, 1st ed., ser. Wiley in Pure and Applied Optics. New York, NY, USA: Wiley, Jan. 1991, pp. 423–459.

[63] R. W. Boyd, *Radiometry and the Detection of Optical Radiation*, ser. Wiley in Pure and Applied Optics. New York, NY, USA: Wiley, Jun. 1983.

[64] R. S. Quimby, "Appendix A: Solid Angle and the Brightness Theorem," in *Photonics and Lasers: An Introduction*. New York, NY, USA: Wiley, 2006, pp. 495–498.

[65] Edmund Optics, "Lens PCX 75 mm diam. $\times$ 75 mm FL MgF_2," 2014. [Online]. Available: http://www.edmundoptics.com/optics/optical-lenses/plano-convex-pcx-spherical-singlet-lenses/mgf2-coated-plano-convex-pcx-lenses/45368/. Accessed on: Jun. 11, 2015.

[66] B. E. A. Saleh and M. C. Teich, "Fourier Optics," in *Fundamentals of Photonics*, 1st ed., ser. Wiley in Pure and Applied Optics. New York, NY, USA: Wiley, Jan. 1991, pp. 108–156.

[67] Thorlabs, "ACL12708U-B – Aspheric Condenser Lens, AR-Coated $650 - 1050$ nm, $D = 1.27$ cm, $f = 8$ mm," Nov. 2013. [Online]. Available: https://www.thorlabs.de/thorcat/CTN/ACL12708U-B-AutoCADPDF.pdf. Accessed on: Apr. 1, 2015.

[68] B. E. A. Saleh and M. C. Teich, "Wave Optics," in *Fundamentals of Photonics*, 1st ed., ser. Wiley in Pure and Applied Optics. New York, NY, USA: Wiley, Jan. 1991, pp. 41–79.

[69] I. S. Gradshteyn and I. M. Ryzhik, *Table of Integrals, Series, and Products*, 7th ed., A. Jeffrey and D. Zwillinger, Eds. New York, NY, USA: Academic, Mar. 2007.